How Charge Regulation Affects pH-Responsive Ampholyte Uptake in Weak Polyelectrolyte Brushes

Keerthi Radhakrishnan, David Beyer, and Christian Holm*

Institute for Computational Physics, University of Stuttgart, D-70569 Stuttgart, Germany

E-mail: holm@icp.uni-stuttgart.de

Abstract

Weak polyelectrolyte brushes are a promising platform for the selective capture and release of charged proteins from bulk solutions. Despite their potential for creating smart responsive surfaces, a detailed microscopic understanding of the uptake behavior in dependence of various parameters remains elusive. In this study, we employ coarse-grained, particle-based simulations to investigate how charge regulation under varying environmental conditions modulate the uptake and release of pH-responsive ampholytes, serving as a toy model for proteins, into weak polyelectrolyte brushes. For quenched brushes with constant ionization, the uptake of ampholytes remains strong across different isoelectric points. In contrast, for weak brushes, the ampholyte uptake becomes selectively sensitive to different isoelectric points and $\mathrm{p}K_\mathrm{A}$-values and exhibits a non-monotonic behavior with changing pH. Enhanced proton partitioning into the brush lowers the *local* pH, significantly shifting the ionization states of both the brush ($\mathrm{p}K_\mathrm{A}^\mathrm{app} > \mathrm{p}K_\mathrm{A}$) and ampholytes ($\mathrm{pI}^\mathrm{app} > \mathrm{pI}$), such that the concurrent ionization of the brush and the ampholyte results in an optimum uptake strength for $\mathrm{p}K_\mathrm{A}^\mathrm{app} < \mathrm{pH} < \mathrm{pI}^\mathrm{app}$. Adjusting the salt concentration broadens the uptake window

and shifts the maximum uptake to higher pH values. Additionally, ampholytes with higher charge regulation capacitance near the isoelectric point demonstrate stronger adsorption, extending selective adsorption capabilities in ampholyte mixtures with similar isoelectric points.

1 Introduction

Polyelectrolytes are chain molecules containing electrically charged groups, which means they are soluble in water and thus interesting materials for many applications in areas such as biomedicine, nutrition, agriculture and cosmetics. A class of polyelectrolytes that have received renewed attention in recent years are weak polyelectrolytes. These are polyelectrolytes which contain titratable, i.e. chemically reactive acid or base groups that can change their ionization state depending on the pH-value and the local (electrostatic) environment.[1] The reversible response of these systems to external stimuli makes them suitable candidates for "smart materials" that can for example be used in targeted drug delivery,[2–4] pH-controlled hydrogel swelling,[5–7] pH-dependent gelation[8] and desalination processes.[9] Similar to synthetic weak polyelectrolytes, many biopolymers like proteins contain weak acidic or basic groups and can thus undergo pH-dependent ionization changes. Proteins often contain both acidic and basic groups, which means that they are "ampholytes" that do not only regulate the magnitude of their charge but can even reverse its sign. Compared to synthetic weak polyelectrolytes, their behavior is further complicated by the diversity of different amino acids and the complex spatial arrangement of the residues within the three-dimensional protein structure. The pH-dependent "charge regulation" of proteins significantly influences their interactions with charged entities such as other proteins[10,11] or synthetic polyelectrolytes[12] and leads to a much richer behavior than is observed in the case of "quenched," i.e. frozen charges. These characteristics can be leveraged in biomedically relevant use cases such as protein detection and purification. For example, in a recent experimental study, nanochambers gated by pH-responsive

polyelectrolyte brushes were used to trap and release proteins.[13] In the past, grafted polyelectrolyte brushes have also been employed to reversibly immobilize proteins in large amounts under certain conditions without hampering their structural and enzymatic integrity,[14–19] which has significant implications for biomedical applications. Works on Bovine Serum Albumin (BSA) interacting with a spherical polyelectrolyte brush reported electrostatically-driven adsorption of BSA into the brush when both are oppositely charged.[14,16] Remarkably, these works demonstrated that protein adsorption happens even on the "wrong side" of the isoelectric point (pI), where the brush and the protein are like-charged. Furthermore, the adsorption strength is profoundly influenced by the ionic strength of the buffer solution.

One proposed explanation of protein adsorption on the wrong side of the isoelectric point is that the proteins have an inhomogeneous distribution of acidic and basic groups on their surface, which results in localized charge patches. As a consequence, even when the net charge of the protein is negative, a positive patch can instigate complexation with a polyanionic brush, concomitant with an entropic counterion release force. This explanation is referred to as the "charge patch argument" and has been corroborated through various experiments,[20,21] simulations,[22,23] as well as theory[24] in the case of patchy proteins. Another rationalization often invoked is the "charge regulation" argument,[25–27] which suggests that due to a higher proton concentration within the dense brush, the local effective pH inside the brush is lower than in the bulk solution. The *local* pH causes a charge reversal of the ampholytic protein inside the brush, making adsorption electrostatically favorable. While there are many works that address the question which mechanism drives the adsorption,[28–32] the answer seems to be system-specific. Hence, any theoretical generalization is challenging, considering the architectural and chemical diversity of proteins.

The theoretical treatment of two-phase systems such as polyelectrolyte brushes requires a proper accounting of the ionic partitioning between the polyelectrolyte-rich phase and the bulk solution. In polyelectrolyte brushes, the densely grafted brush acts as a polymer-rich "brush-phase," while the surrounding ionic solution acts as a

"bulk-phase." Imposing the electroneutrality of both phases and establishing chemical equilibria for the small ions between them gives rise to a Donnan potential and an enhanced partitioning of counterions into the brush. In a weak polyelectrolyte brush, the reversible ionization of the acidic or basic groups of the brush is affected by the *local* pH within the system. This ionization state of the polyelectrolyte affects in turn the partitioning of ions (including H^+) between the system and the reservoir and thus the *local* pH within the system, leading to a complex coupling between ionization and ion partitioning. Further complications arise due to (electrostatic) interactions, which can lead to a strongly non-ideal ionization behavior, the so-called "polyelectrolyte effect." [33] Accounting for all of these effects is crucial for a consistent theoretical description of the charge-based sequestration of pH-responsive ampholytes such as proteins. A popular class of brush models are based on the mean field approximation, which allows for fast and efficient calculations.[34–36,36–41] However, mean field models fail to capture electrostatic interactions in their entirety, especially for the case of multivalent entitites, where correlation effects become important.[42–49]

In contrast to the limitations of mean-field approaches, recent advances in simulation methodology allow for simulations of charge-regulating two-phase systems on a particle-based level, accounting for the full electrostatic interactions and charge regulation effects at the same time.[33] Here, we employ this particle-based simulation approach to study the tunable and reversible binding of pH-responsive ampholytes to a weak polyelectrolyte brush. In the context of protein sequestration, a proper quantification of the uptake and release of specific proteins by a polyelectrolyte brush necessitates modeling several features such as the specific distribution of titrable groups on the protein surface, including cooperative ionization,[10,11,20] non-electrostatic, short-range attractive interactions[26] and steric interactions. Considering the multifaceted nature of the problem and the fact that there is no holistic way to address all of these aspects simultaneously, a viable strategy to attack the problem is a bottom-up approach, where one starts with a simplified model, adding further complexity step-by-step. Adhering to this idea, in the current work we investigate how the acid-base equilibrium

of a weak polyelectrolyte brush and the concomitant partitioning of ions dictate the charge regulation and uptake of a small ampholyte molecule. We employ a simple coarse-grained representation of a weakly ampholytic molecule that can dynamically adjust its charge depending on the (*local*) pH. This construction allows us to solely focus on the monopolar contribution of the charge regulation aspect, neglecting further complications arising from the complex charge distribution of real proteins. In a follow-up work, we will increase the complexity by introducing more realistic protein models with asymmetric charge group distributions, accounting for dipolar and charge patch-induced effects as well as steric interactions. The outlined approach enables us to focus on generic features of the system that are independent of a specific protein, thus allowing us a to gain a general understanding of pH-reponsive protein uptake by brushes and guide future experiments.[50,51]

2 Simulation Model and Methods

Similar to our previous studies,[49,52] we carry out coarse-grained, particle-based simulations of a weak polyelectrolyte brush in contact with a reservoir, using a hybrid MD/MC scheme. All simulations are performed using version 4.2.0 of the simulation software package ESPResSo.[53,54] In the following, we describe the employed model and simulation methodology.

2.1 Coarse-Grained Model

We use a coarse-grained, implicit solvent model of a weak polyelectrolyte brush. The generic bead-spring model is based on the popular polymer model of Kremer and Grest,[55] in which all particles, i.e. monomers, small ions and ampholytes, interact via

a truncated Lennard-Jones potential:

$$V_{\text{LJ-cut}}(r) = \begin{cases} 4\epsilon_{\text{LJ}} \left(\left(\frac{\sigma}{r}\right)^{12} - \left(\frac{\sigma}{r}\right)^{6} \right) - 4\epsilon_{\text{LJ}} \left(\left(\frac{\sigma}{r_{\text{cut}}}\right)^{12} - \left(\frac{\sigma}{r_{\text{cut}}}\right)^{6} \right) & \text{if } r \leq r_{\text{cut}} \\ 0 & \text{if } r > r_{\text{cut}}. \end{cases} \tag{1}$$

Here, σ is the particle diameter with a value of $\sigma = 0.355\,\text{nm}$ and r_{cut} is the cutoff distance of the potential. Except for the case of non-electrostatic attractions between ampholytes and monomers ($r_{\text{cut}} = 2.5\,\sigma$), we always use a purely repulsive potential ($r_{\text{cut}} = 2^{\frac{1}{6}}\,\sigma$), corresponding to the Weeks-Chandler-Andersen (WCA) potential.[56] If not mentioned otherwise, we set the interaction strength to a value of $\epsilon_{\text{LJ}} = k_{\text{B}}T$, where $T = 298.15\,\text{K}$ corresponds to room temperature. The covalent bonds between adjacent monomers in the chains are considered to be non-linear springs, described by the Finite Extensibility Nonlinear Elastic (FENE) potential:[55]

$$V_{\text{FENE}}(r) = \begin{cases} -\frac{k\Delta r_{\text{max}}^2}{2} \ln\left(1 - \left(\frac{r - r_0}{\Delta r_{\text{max}}}\right)^2\right) & \text{if } r \leq \Delta r_{\text{max}} \\ \infty & \text{if } r > \Delta r_{\text{max}}. \end{cases} \tag{2}$$

In the current study, we set the maximum extension of the bond to a value of $\Delta r_{\text{max}} = 2.0\,\sigma$, the spring constant to $k = 30\,k_{\text{B}}T/\sigma^2$ and the equilibrium length of the bonded potential to $r_0 = 0$. Electrostatic interactions are treated on the level of a restricted primitive model (RPM). This means that all charged particles interact via the full Coulomb potential

$$V_{\text{Coulomb}}^{ij}(r) = \frac{\lambda_{\text{B}} k_{\text{B}} T z_i z_j}{r}, \tag{3}$$

where z_i and z_j are the valencies of the respective particles. The strength of the interaction is controlled by the Bjerrum length $\lambda_{\text{B}} = e^2/4\pi\epsilon k_{\text{B}}T$, which corresponds to the distance at which the interaction energy between two monovalent ions is equal to the thermal energy. Equation 3 models the solvent only implicitly, i.e. via an effective dielectric constant that is contained in the Bjerrum length. In order to mimic

an aqueous solution at room temperature, we set $\lambda_B = 2\,\sigma = 7.1\,\text{Å}$. To account for the long-range nature of the Coulomb interaction in our simulations, we use the P^3M method,[57,58] complemented by the electrostatic layer correction (ELC)[59,60] to correctly model the geometry of the 2D-periodic slab system.

The described interaction potentials allow us to build up a coarse-grained representation of a weak polyelectrolyte brush as shown in Fig. 1 (a). Our brush consists of 5×5 chains of length $N = 25$, which are uniformly grafted to a flat surface at $z = 0$ with a grafting density of $\Gamma = 0.1\,\sigma^{-2}$. This grafting is achieved by tethering one end of each chain at a fixed position on the wall, which is impenetrable to all particles due to a repulsive WCA interaction. In the directions parallel to the interface, labeled x and y in the following, we employ periodic boundary conditions, while in the perpendicular z-direction, the system is confined by hard walls at $z = 0$ and $z = 150\,\sigma$.

2.2 Methodology

We use Langevin dynamics at a temperature of $T = 298.15\,\text{K}$, with a friction coefficient of $\gamma = 1.0$ (in LJ units) and a reduced mass $m = 1.0$ to sample different conformational states of the system at a fixed chemical composition. The stochastic equations of motion are numerically integrated using the Velocity-Verlet method[61] with an integration time step of $\Delta t = 0.01\,\sigma\,(m/k_BT)^{1/2}$. Additionally, we explicitly consider the effects of charge regulation, i.e. of the chemical equilibria corresponding to the weak polyelectrolyte brush and other pH-responsive entities present in the system. On the coarse-grained level, such chemical equilibria are conveniently modeled using Monte Carlo approaches.[1,62–66] Here, we employ a generalized version[67] of the grand-reaction method,[33,66,68] which models a polyelectrolyte phase that is grand-canonically coupled to a reservoir containing small ions, as shown schematically in Fig. 1 (b). This method, originally developed for the simulation of weak polyelectrolyte hydrogels,[6,7] has been applied to a wide range of systems, including the dialysis of weak polyelectrolyte chains,[33] polyelectrolyte complex coacervates[8,69] and grafted polyelectrolyte brushes.[49,52,70,71] For the present system, we have to consider two different chemical

reactions: on the one hand, the weak acidic monomers HA of the brush can dissociate in the reaction

$$\mathrm{HA} \rightleftharpoons \mathrm{A}^- + \mathrm{H}^+, \tag{4}$$

which is described by the equilibrium constant $K_\mathrm{A} = 10^{-\mathrm{p}K_\mathrm{A}}$. Here, we set $\mathrm{p}K_\mathrm{A} = 4.0$, which corresponds to polyacrylic acid, a weak polyelectrolyte commonly employed in experiments to synthesize pH-responsive brushes.[14–16,18] On the other hand, the system also contains small ampholytes, denoted by Ha in their neutral state. These ampholytic particles can react as an acid,

$$\mathrm{Ha} \rightleftharpoons \mathrm{a}^- + \mathrm{H}^+, \tag{5}$$

described by the equilibrium constant $K_\mathrm{a}^\mathrm{acid} = 10^{-\mathrm{p}K_\mathrm{a}^\mathrm{acid}}$ and as a base,

$$\mathrm{H_2a}^+ \rightleftharpoons \mathrm{Ha} + \mathrm{H}^+, \tag{6}$$

described by the equilibrium constant $K_\mathrm{a}^\mathrm{base} = 10^{-\mathrm{p}K_\mathrm{a}^\mathrm{base}}$. In our coarse-grained description, the ampholytic particles are modeled as a single bead, i.e. apart from the ionization state we neglect any internal structure and thus also dipoles and higher multipole moments. Contrasting with the weak acidic monomers constituting the brush, we do not restrict $\mathrm{p}K_\mathrm{a}^\mathrm{acid}$ and $\mathrm{p}K_\mathrm{a}^\mathrm{base}$ to fixed values but systematically vary their difference

$$\Delta\mathrm{p}K_\mathrm{a} \equiv \mathrm{p}K_\mathrm{a}^\mathrm{acid} - \mathrm{p}K_\mathrm{a}^\mathrm{base} \tag{7}$$

in order to investigate the effects of charge regulation. Furthermore, we vary the isoelectric point, given by

$$\mathrm{pI} \equiv \frac{\mathrm{p}K_\mathrm{a}^\mathrm{acid} + \mathrm{p}K_\mathrm{a}^\mathrm{base}}{2}, \tag{8}$$

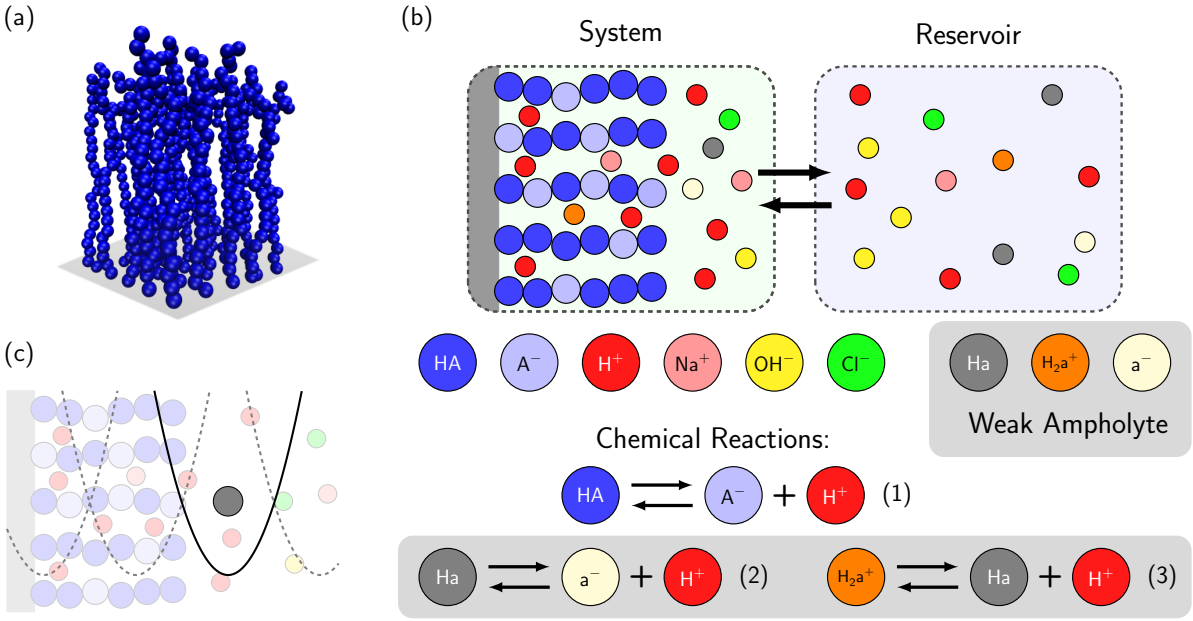

Figure 1: (a): Simulation snapshot of the employed brush model. Small ions are not shown for clarity. (b): Schematic representation of the grand-reaction ensemble employed in this study.[33,67,68] The "system" phase, containing the weak polyelectrolyte brush consisting of monomers HA, is grand-canonically coupled to a reservoir at a given pH-value that additionally contains salt (NaCl) and ampholytes (Ha). The weak ampholyte Ha can protonate and deprotonate into H_2a^+ and a^-, respectively (grey background). Equation (1) depicts the chemical reaction of the brush monomers while (2) and (3) show the acidic and basic reaction of the ampholyte, respectively. (c): Schematic of the umbrella sampling method for a single ampholyte interacting with a brush. The harmonic biasing potential is shown as a black line, biasing potentials at other positions are shown as dashed lines.

which corresponds to the pH-value at which the ampholyte is electroneutral. We restrict ourselves to the case $\Delta pK_a \geq 0$, since the opposite case, corresponding to ampholytic particles that exist in a zwitterionic state at intermediate pH-values, is not properly captured by our simplified model due to the neglect of the internal structure of the ampholyte.

As shown in Fig. 1 (b), the grand-reaction method considers a system that is grand-canonically coupled to an aqueous solution of ions and ampholytic particles, termed the "reservoir." In the case of a weak polyelectrolyte brush, the reservoir corresponds to the bulk solution far away from the brush,[52] and for the present system, its composition is determined by the pH-value pH^{res}, the salt concentration c_{salt} and

the total concentration of dissolved ampholytic particles $c_{\mathrm{Ha}}^{\mathrm{res},0}$. We assume that the pH-value of the reservoir is set by adding an appropriate amount of a strong acid (HCl) or base (NaOH) to the solution. Furthermore, it is important to note that the relative fractions of Ha, a^-, $\mathrm{H_2a}^+$ are not known a-priori, but are a non-trivial consequence of the ionization equilibrium in the reservoir. The grand-reaction method models the chemical reactions given by Equation 4, Equation 5 and Equation 6, as well as the exchange of small ions, which can be formally represented by a set of "virtual" chemical reactions:

$$\emptyset \rightleftharpoons \mathrm{X}^+ + \mathrm{X}^- \tag{9}$$

$$\emptyset \rightleftharpoons \mathrm{H_2a}^+ + \mathrm{X}^- \tag{10}$$

$$\emptyset \rightleftharpoons \mathrm{X}^+ + \mathrm{a}^- \tag{11}$$

$$\emptyset \rightleftharpoons \mathrm{Ha}. \tag{12}$$

Here, X^+ can stand for Na^+ or H^+ and X^- represents Cl^- or OH^-. The equilibrium constants of these electroneutrality conserving reactions are determined by the chemical potentials of the various species in the reservoir. In general, the mapping between the reservoir composition and the equilibrium constants is non-trivial and requires additional simulations,[67] as explained in the ESI (section 1). Once the required values of the equilibrium constants have been determined, the set of reactions is sampled using the established Reaction-Ensemble Monte Carlo method (RxMC)[63,64] with a Monte Carlo acceptance probability given by

$$P_{\mathrm{n,o}}^{\mathrm{RxMC}} = \min\left\{1, \left(\prod_i \frac{N_i^0!\,(Vc^{\ominus})^{\nu_i\xi}}{(N_i^0+\nu_i\xi)!}\right)\exp\left(\beta\left[\xi\sum_i \nu_i(\mu_i-\mu_i^{\ominus}) - \Delta\mathcal{U}_{\mathrm{n,o}}\right]\right)\right\}. \tag{13}$$

In this equation, $\Delta\mathcal{U}_{\mathrm{n,o}}$ is the change in potential energy between the old (o) and the proposed new (n) state, ξ is the extent of reaction, β is the inverse temperature, ν_i the stoichiometric coefficient of species i and μ_i the corresponding chemical potential. We perform equilibration runs for a total of 10^5 integration steps, with 50 reaction steps

performed every 100 integration steps. The production runs consist of a total of 2×10^6 integration steps with 50 reaction trials every 100 integration steps.

Additional information about the interaction between the brush and the ampholytes can be obtained from the potential of mean force (PMF) $\Delta\Omega(z)$, which describes the effective interaction of a single ampholyte with the brush at a given distance z, averaged over different chain conformations, ion positions and ionization states. The symbol Ω is used to stress that the PMF is not a Helmholtz free energy but a semi-grand canonical potential. In simulations, the PMF can be obtained using enhanced sampling methods.[61] Here, we opt for the umbrella sampling method,[72,73] which constrains the ampholyte in a harmonic biasing potential (cf. Fig. 1 (c)). By carrying out multiple simulations at different distances of this harmonic potential from the brush and analyzing the data using the Weighted Histogram Analysis Method (WHAM),[74,75] we can thus obtain the PMF. We choose a spacing of 0.5 σ along the reaction coordinate and a spring constant of $k_{\mathrm{umbrella}} = 3\,k_{\mathrm{B}}T/\sigma^2$ for the harmonic potential. For each distance, we perform a total of 10^5 integration steps for equilibration and 10^6 for the production run. Every 100 integration steps, we perform 50 reaction moves.

3 Results

3.1 Titration behavior

Before we study the interaction of ampholytes with a weak polyelectrolyte brush, we briefly consider these two entities independently. For this purpose, we investigate the ionization behavior of a weak polyelectrolyte brush in equilibrium with a salt solution as well as the ionization behavior of the ampholytes in a salt solution.

Fig. 2 (a) shows the degree of ionization $\alpha \equiv c^{\mathrm{sys}}_{\mathrm{A}^-}/(c^{\mathrm{sys}}_{\mathrm{A}^-} + c^{\mathrm{sys}}_{\mathrm{HA}})$ of the polyelectrolyte brush as a function of the pH in the reservoir for various salt concentrations. A comparison with the ideal titration behavior of a weak acid (in dashed line) as described by the Henderson-Hasselbalch equation, $\alpha = (1 + 10^{\mathrm{p}K_{\mathrm{A}} - \mathrm{pH}})^{-1}$, reveals a

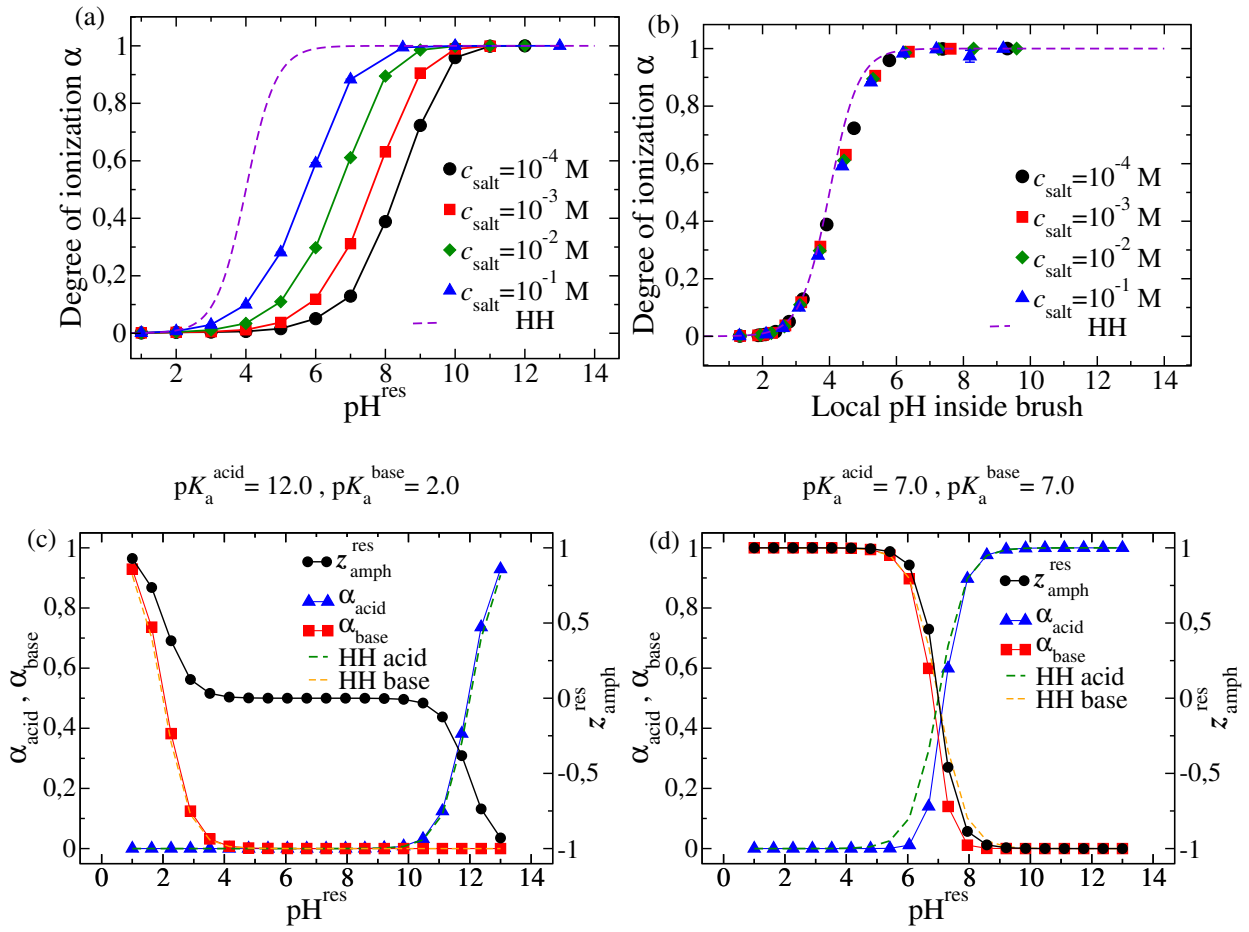

Figure 2: **Titration curve of the brush:** (a) Degree of ionization (α) of the polyelectrolyte brush as a function of the pH in the reservoir ($\mathrm{pH^{res}}$) for varying salt concentrations. The dashed line represents the corresponding ideal curve described by the Henderson-Hasselbalch (HH) equation. (b) Shifted ionization curve of the brush (solid symbols) with respect to the local pH inside the brush. **Titration curve of weak ampholyte:** (c) and (d): Degree of ionization vs. reservoir pH ($\mathrm{pH^{res}}$) of the acidic part of the ampholyte (α_{acid}), shown with blue triangles (y-axis on the left), and the basic part of the ampholyte (α_{base}), shown with red squares (y-axis on the left). Dashed lines depict the ideal HH acid (in green) and HH base (in orange) curves. The net average charge of the ampholyte ($z^{\mathrm{res}}_{\mathrm{amph}}$) is shown with black circles (y-axis on the right). (c) corresponds to the case of $\mathrm{p}K_{\mathrm{a}}^{\mathrm{acid}}$=12.0 and $\mathrm{p}K_{\mathrm{a}}^{\mathrm{base}}$=2.0, and (d) is for $\mathrm{p}K_{\mathrm{a}}^{\mathrm{acid}}$=7.0 and $\mathrm{p}K_{\mathrm{a}}^{\mathrm{base}}$=7.0.

marked $\mathrm{p}K_{\mathrm{A}}$-shift in the ionization behavior that increases as the salt concentration is lowered. Polyelectrolyte brushes constitute a two-phase system with a "brush-phase" containing polyelectrolyte chains and a surrounding "bulk-phase" that contains only small ions. In an ideal system, imposing the condition of electroneutrality and chemical equilibria between these phases, gives rise to a Donnan partitioning of ions. Here, de-

pending on the concentration of impermeable ions and the ionic strength, an enhanced concentration of cations (including H+) is seen in the system than the reservoir. The enhanced partitioning of H+ ions causes a lowering of the *local* effective pH inside the brush which affects the ionization state of the weak PE brush. In addition to this Donnan effect, in the non-ideal case the electrostatic interactions within the brush affect the ionization of the chains as well, the so-called "polyelectrolyte effect". Hence, the shift in the ionization seen in Fig. 2 (a) is caused by a combination of "polyelectrolyte effect" and the Donnan effect, with the latter dominating in the case of densely grafted brushes.[6,7,33,52] By plotting the degree of ionization as a function of the *local* pH within the brush (shown in Fig. 2 (b)), the Donnan effect can be effectively subtracted, leading to an ionization curve that almost coincides with the ideal prediction. The small remaining shift is caused by electrostatic interactions. However, at lower grafting densities, although the Donnan effect weakens, a substantial ionization shift still occurs due to the electrostatic interactions. After correcting for the *local* pH, the ionization curve does not fully revert to the ideal prediction; instead, a significant deviation remains, driven by the "polyelectrolyte effect".

For the ampholytes, we have to distinguish the degree of ionization of the acid, given by $\alpha_{\mathrm{acid}} \equiv c^{\mathrm{res}}_{\mathrm{a}^-}/c^{\mathrm{res},0}_{\mathrm{Ha}}$ and the degree of ionization of the base, given by $\alpha_{\mathrm{base}} \equiv c^{\mathrm{res}}_{\mathrm{H2a}^+}/c^{\mathrm{res},0}_{\mathrm{Ha}}$. The average net charge of the ampholyte, $z^{\mathrm{res}}_{\mathrm{amph}}$, can accordingly be expressed as $z^{\mathrm{res}}_{\mathrm{amph}} = e(\alpha_{\mathrm{base}} - \alpha_{\mathrm{acid}})$, with the elementary charge e. Fig. 2 (c) and (d) show the quantities α_{acid}, α_{base} and $z^{\mathrm{res}}_{\mathrm{amph}}$ for $\mathrm{p}K^{\mathrm{acid}}_{\mathrm{a}} = 2.0$, $\mathrm{p}K^{\mathrm{base}}_{\mathrm{a}} = 12.0$ (c) and $\mathrm{p}K^{\mathrm{acid}}_{\mathrm{a}} = \mathrm{p}K^{\mathrm{base}}_{\mathrm{a}} = 7.0$ (d). In the case $\mathrm{p}K^{\mathrm{acid}}_{\mathrm{a}} \gg \mathrm{p}K^{\mathrm{base}}_{\mathrm{a}}$ (subfigure (c)), the ionization steps of the acid and the base are completely decoupled. Because in the concentration regime considered here, electrostatic interactions are of minor importance, the resulting charge $z^{\mathrm{res}}_{\mathrm{amph}}$ is well-described by a simple superposition of the Henderson-Hasselbalch equation for the acid and the base and changes from $+1$ to -1 with increasing pH. The broad plateau at intermediate pH-values results from the negligibly small ionization of both the acid and the base, resulting in neutral ampholytic particles. In contrast, for the case $\mathrm{p}K^{\mathrm{acid}}_{\mathrm{a}} = \mathrm{p}K^{\mathrm{base}}_{\mathrm{a}}$ (subfigure (d)) the coupling between the ionization of the

acid and the base leads to a slight suppression in the ionizations compared to a naive application of the Henderson-Hasselbalch equation. Importantly, due to the concurrent ionization of the acid and the base near the isoelectric point, in this case the titration curve is much steeper. This behavior corresponds to a pronounced charge regulation effect near the isoelectric point.

3.2 Uptake of Ampholytes by the Brush

Now we investigate the uptake behavior of ampholytes by the brush at a range of conditions. To gain a holistic understanding of the influence of various factors, we systematically vary external conditions (pH and salt concentration) as well as material parameters (acidity constants and short-range attractions). We quantify the uptake in terms of the partition coefficient of the ampholytes between the brush phase and the reservoir. The partition coefficient of any species i is defined as the ratio of the concentration of this species in the system and the reservoir,

$$\xi_i \equiv c_i^{\mathrm{sys}}/c_i^{\mathrm{res}}.$$

Since we model the brush-solution interface explicitly, in our case, the monomer concentration fairly remains homogeneous throughout the brush bulk, with only slight peak at distances very close to the wall and a sharp decrease at the brush-solution interface (cf. Fig.S2 in the ESI). This in turn results in a homogeneous partitioning of ions across the brush interior (cf. Fig. S3 in the ESI). It is evident from the ionic partitioning profiles that the partitioning attains a maximum and remains almost constant for $z \lesssim R_{\mathrm{e}}$, where R_{e} is the average end-to-end distance of the tethered polymers, followed by a rapid decay towards the brush boundary. Consequently, we define the partition coefficient of ampholytes as

$$\xi_{\mathrm{amph}} \equiv \frac{c_{\mathrm{amph}}^{\mathrm{brush}}}{c_{\mathrm{amph}}^{\mathrm{res}}} = \frac{N_{\mathrm{amph}}^{(z<R_{\mathrm{e}})}/(L_{\mathrm{x}}L_{\mathrm{y}}R_{\mathrm{e}})}{c_{\mathrm{amph}}^{\mathrm{res}}}, \tag{14}$$

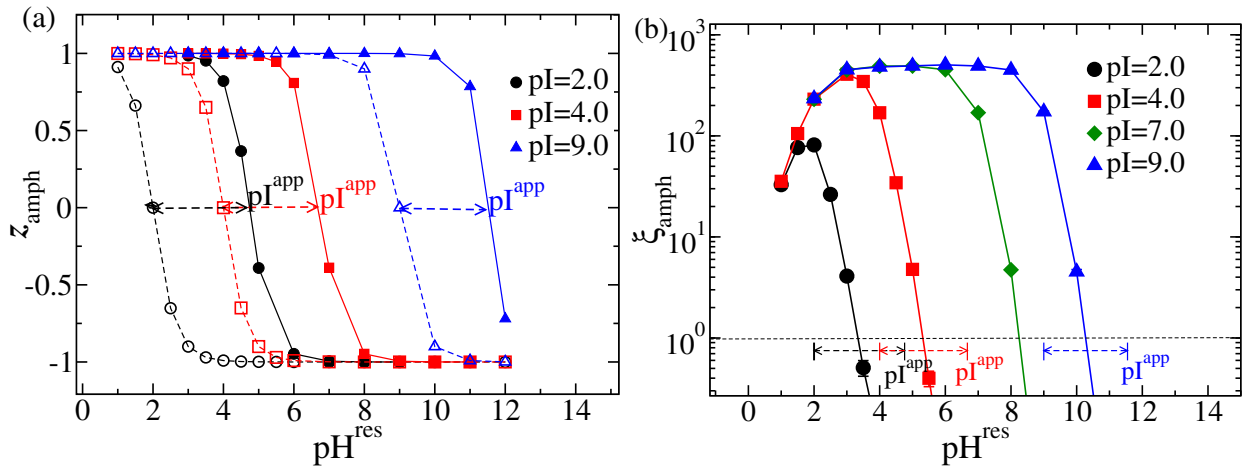

Figure 3: (a): Average net charge of the ampholyte in the reservoir ($z^{\mathrm{res}}_{\mathrm{amph}}$), shown with open symbols and dashed line, and average net charge of the ampholyte within the brush ($z^{\mathrm{brush}}_{\mathrm{amph}}$), shown with solid symbols and solid line, as a function of the pH in the reservoir ($\mathrm{pH}^{\mathrm{res}}$) for ampholytes of varying pI. (b): Ampholyte uptake (ξ_{amph}) in a quenched brush as a function of the pH in the reservoir ($\mathrm{pH}^{\mathrm{res}}$) for different isoelectric points pI. The dashed lines with arrows on both ends indicate the pH range ($\mathrm{pI} - \mathrm{pI}^{\mathrm{app}}$) where the ampholyte undergoes a charge reversal. The parameters chosen in both subfigures are $\Delta \mathrm{p}K_{\mathrm{a}} = 0$ and $c_{\mathrm{salt}} = 10^{-2}\,\mathrm{M}$, $c^{\mathrm{res},0}_{\mathrm{Ha}} = 10^{-4}\,\mathrm{M}$.

where $N^{(z<R_{\mathrm{e}})}_{\mathrm{amph}}$ denotes the total number of ampholytic particles at a distance $z < R_{\mathrm{e}}$ from the wall.

3.2.1 Uptake in Quenched Brushes

Before introducing charge regulation of the brush, we focus on the simpler case of a quenched (strong) polyelectrolyte brush, which means that the brush is always fully ionized, irrespective of the pH-value. Furthermore, the reaction constants of the ampholytes are always chosen as $\mathrm{p}K^{\mathrm{acid}}_{\mathrm{a}} = \mathrm{p}K^{\mathrm{base}}_{\mathrm{a}}$, such that the charge regulation capacitance near the isoelectric point for all combinations remains the same, with only the isoelectric point shifting. Because the ionization state of the quenched brush is not affected by the pH, the uptake behavior is thus solely dictated by the net charge of the ampholytes and the overall ionic strength. Fig. 3 (a) shows the average charge of an ampholyte in the reservoir ($z^{\mathrm{res}}_{\mathrm{amph}}$) and the average charge of the ampholyte upon adsorption into the brush ($z^{\mathrm{brush}}_{\mathrm{amph}}$) in response to changing $\mathrm{pH}^{\mathrm{res}}$ for ampholytes of varying pI. The ionization of the ampholytes inside the brush is estimated using the *local*

pH inside the brush. This estimation is in agreement with the net charge evaluated directly from adsorbed ampholytes (cf. Fig. S5 in the ESI). However, the latter gives no statistically reliable values for the ampholyte charge inside the brush for higher pH, where no uptake happens. Comparing the ionization curves in the reservoir and the brush, we observe in all cases a similar shift of the isoelectric point, $\mathrm{pI}^{\mathrm{app}} = \mathrm{pI} + \Delta\mathrm{pH}$, upon adsorption into the brush, with $\Delta\mathrm{pH} \approx 2.7$. Thus, in a window of approximately ΔpH beyond the isoelectric point, adsorption into the brush is accompanied by a charge reversal of the ampholyte from negative to positive. Consequently, one expects a large uptake of ampholytes for $\mathrm{pH}^{\mathrm{res}} < \mathrm{pI}^{\mathrm{app}}$, with a sharp decrease around $\mathrm{pH}^{\mathrm{res}} \approx \mathrm{pI}^{\mathrm{app}}$. Beyond $\mathrm{pI}^{\mathrm{app}}$, the uptake should vanish almost completely due to the like charge of the brush and the ampholyte. The observed pH shift, in case of quenched brushes can be understood in the context of the Donnan model.[52] According to ideal Donnan theory, the proton concentration inside the brush and thus the local pH shift within the brush depends on the ratio of the brush's charge density (c_{A^-}) and the ionic strength (I^{res}) in the reservoir:[52]

$$\Delta\mathrm{pH} \overset{\text{ideal}}{=} \log_{10}\left(\frac{c_{\mathrm{A}^-}}{2I^{\mathrm{res}}} + \sqrt{\left(\frac{c_{\mathrm{A}^-}}{2I^{\mathrm{res}}}\right)^2 + 1}\right)$$

For a quenched brush, the charge density remains constant with changing pH. However, the ionic strength in the reservoir changes with pH, but for a given salt concentration, it largely remains constant for a wide intermediate pH range (see ESI Fig.S1). Resultantly, quenched brushes exhibit a nearly constant ΔpH shift in ionization across different pH values. Like for the present case with $c_{\mathrm{A}^-} \approx 5\,\mathrm{M}$ and $I^{\mathrm{res}} = 10^{-2}\,\mathrm{M}$, the predicted pH shift from the Donnan model gives $\Delta\mathrm{pH} \approx 2.7$, and closely matches with the observed pH shift. While this behavior is consistent across most pH levels, deviations from the characteristic plateau in ionic strength at extreme pH (see ESI Fig.S1), might lead to change in the local pH shift as well. Nevertheless, for strongly grafted brushes, the constant pH shift remains valid as long as ionic strength remains relatively invariant under changing pH, and can be predicted from the ideal Donnan

shift.[52]

Furthermore, this expected window of favorable uptake is in general agreement with the uptake behavior observed in the simulations, as shown in Fig. 3 (b). In all cases, we observe a window of substantial uptake at intermediate pH-values, while the uptake diminishes at extreme pH-values. Furthermore, we find that the size of the window is strongly dependent on the chosen value of the isoelectric point pI. The substantial uptake seen beyond the isoelectric point in each case can be attributed to the described shift of the isoelectric point and charge reversal upon adsorption. However, it is important to note that the boundary of the uptake window lies below the value of $\mathrm{pI}^{\mathrm{app}}$ in all cases, which suggests that charge reversal alone is not sufficient for ampholyte uptake beyond the isoelectric point. Additionally, there are deviations from the maximum uptake at lower pH-values ($\mathrm{pH}^{\mathrm{res}} < 3.0$). This effect stems from the increase in the ionic strength of the reservoir at extreme pH-values (cf. Fig. S1 in the ESI). As a result, the Donnan effect and thus the partitioning of cations weaken in these limits.[33,52]

3.2.2 Uptake in Annealed Brushes

Now we introduce charge regulation of the brush, i.e. we consider the uptake of ampholytes into an annealed (pH-responsive) polyelectrolyte brush with $\mathrm{p}K_{\mathrm{A}} = 4.0$. In Fig. 4 (a), we show the charge on the ampholyte in the reservoir ($z^{\mathrm{res}}_{\mathrm{amph}}$) and within the brush ($z^{\mathrm{brush}}_{\mathrm{amph}}$) for different values of the isoelectric point. For a comparative analysis of the change in the charge of the brush and the ampholyte, we also plot the ideal prediction for the degree of ionization $\alpha_{\mathrm{brush,ideal}}$ of the brush and the actual degree of ionization α_{brush}. There are major differences to the case of a quenched brush. Firstly, similar to the case of the isolated brush above, the brush ionization itself varies with pH and undergoes a $\mathrm{p}K_{\mathrm{A}}$ shift due to the coupled Donnan and polyelectrolyte effects. Secondly, a non-uniform pI-shift of the ampholyte inside the brush is seen across different isoelectric points, with $\mathrm{pI} = 2.0$ undergoing a minimal shift compared to the other cases. This happens, because in weak brushes the strength of the Donnan effect

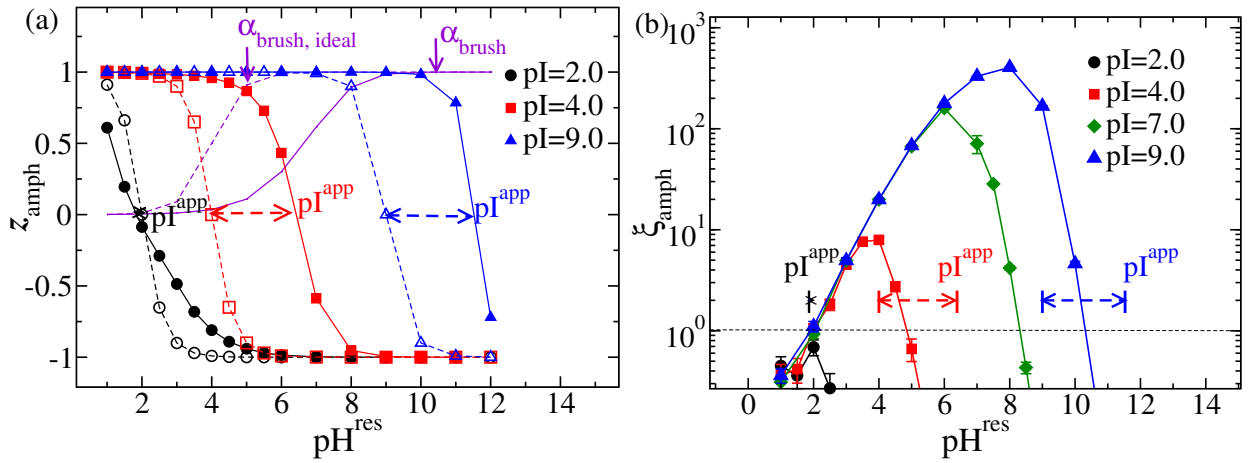

Figure 4: (a): Average net charge of the ampholyte in the reservoir ($z^{\mathrm{res}}_{\mathrm{amph}}$), shown with open symbols and dashed line, and average net charge of the ampholyte within the brush ($z^{\mathrm{brush}}_{\mathrm{amph}}$), shown with solid symbols and solid line, as a function of the pH in the reservoir ($\mathrm{pH}^{\mathrm{res}}$) for ampholytes of varying pI. $\alpha_{\mathrm{brush,ideal}}$ is the ideal degree of ionization of the brush (Henderson-Hasselbach), α_{brush} is the degree of ionization of the brush obtained from the simulation. (b): Ampholyte uptake (ξ_{amph}) in an annealed brush as a function of the pH in the reservoir ($\mathrm{pH}^{\mathrm{res}}$) for different isoelectric points pI. The dashed lines with arrows on both ends indicate the pH range ($\mathrm{pI} - \mathrm{pI}^{\mathrm{app}}$) where the ampholyte undergoes a charge reversal. The parameters chosen in both subfigures are $\Delta \mathrm{p}K_{\mathrm{a}} = 0$ and $c_{\mathrm{salt}} = 10^{-2}\,\mathrm{M}$.

strongly varies with the reservoir pH. At low pH values, when the brush is uncharged, there is a minimal Donnan effect and consequently, the pH inside the brush and the bulk are approximately equal. However, with increasing pH in the bulk, the chains ionize more, leading to a pronounced Donnan effect (and lower $\mathrm{pH}^{\mathrm{brush}}$). At very high pH-values, this shift decreases again due to the increased ionic strength (cf. Fig. S4 in the ESI).

To study the partitioning behavior, we show in Fig. 4 (b) the partition coefficient of ampholytes. In comparison to the quenched brush (cf. Fig. 3 (b)), the pH-window in which a significant uptake of ampholytes into the brush happens is now much smaller, with a lower uptake at low pH-values. By comparing the uptake behavior with the ionization (Fig. 4 (a)), it can inferred that in the case of a weak polyelectrolyte brush the ampholyte uptake is dictated both by the pH-response of the brush and the ampholyte itself. In the present case, the apparent $\mathrm{p}K_{\mathrm{A}}$-value of the brush is around 6.5, and only for $\mathrm{pH}^{\mathrm{res}} \gtrsim 4.0$ the chains begin to obtain a noticeable charge.

Thus, the pK_A^{app} of the brush and the pI^{app} of the ampholyte determine the size of the pH-window in which one expects a significant uptake. For example, in the case pI = 2.0, we have $pI^{app} < 4.0$, suggesting that there is no window of pH where the ampholyte is positive while the brush is negative. Hence, no adsorption ($\xi_{amph} > 1$) is seen for the whole pH range in this case. In contrast, for ampholytes with pI = 4.0 and pI = 9.0, there is a substantial window between the pH where the polyanionic brush starts ionizing and the shifted isoelectric point (pI^{app}), where uptake is favorable due to the electrostatic attraction. Therefore, in those cases, roughly in the window of $4.0 < pH < pI^{app}$, we expect an uptake of ampholyte by the brush. As the pH-value is increased, initially the uptake grows due to the increasing ionization of the chain. At some point, the uptake should reach a maximum and decrease again, now due to the decreasing partial positive charge of the ampholyte. For pH-values beyond pI^{app}, the uptake should vanish, since charge reversal of the ampholyte does not happen anymore. The overall uptake behavior obtained from the simulations, shown in Fig. 4 (b), is in agreement with this picture. However, like in the case of quenched brushes, the pH window in which charge reversal is observed (between pI and pI^{app}) is broader than the pH window in which a substantial uptake happens. This shows again that charge reversal alone is not sufficient for uptake favourability. Furthermore, we observe that the maximum uptake strength for an ampholyte into an annealed brush increases with the isoelectric point pI, contrary to the case of a strong brush. This behavior arises due to the competition between the growing partial negative charge of the brush and the diminishing partial positive charge of the ampholyte with increasing pH. In the case $pI = 9.0 \gg pK_A^{app}$, there exists an overlapping window of pH where both the brush and the ampholyte are fully ionized to $\alpha^{brush} = 1$ and $z_{amph}^{brush} = -1$. In that case the maximum uptake strength becomes similar to that seen in the case of a quenched brush. Our observations suggest that the use of weak brushes enhances the tunability of both the window of adsorption/desorption, as well as the strength of uptake with changing pH as compared to strong brushes. Moreover, weak brushes provide better selectivity of adsorption depending on the pI of the ampholyte and the pK_A of the

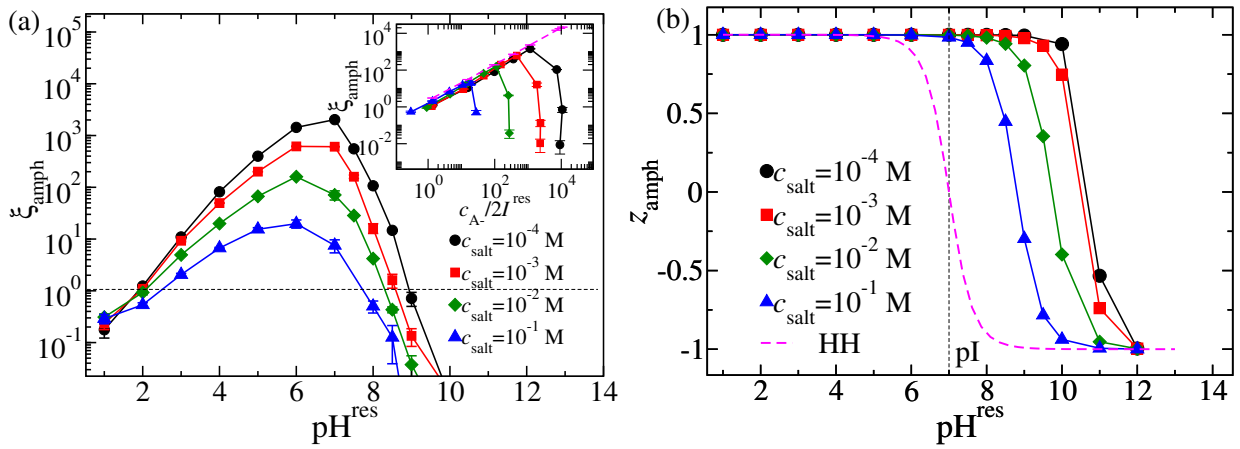

Figure 5: (a): Ampholyte uptake (ξ_{amph}) in an annealed brush as a function of the pH in the reservoir (pH^{res}) for different salt concentrations. (Inset) Ampholyte uptake (ξ_{amph}) plotted as a function of ratio of concentration of impermeable A^- ions to the ionic strength in the reservoir ($c_{A^-}/2I^{\text{res}}$), for different salt concentrations as in main plot. The dashed pink line corresponds to the ideally predicted counterion partitioning by Donnan theory. (b): Average net charge of the ampholyte in the reservoir ($z^{\text{res}}_{\text{amph}}$) shown in dashed line and average net charge of the ampholyte within the brush ($z^{\text{brush}}_{\text{amph}}$), shown with solid symbols, as a function of the pH in the reservoir (pH^{res}). The parameters chosen in both subfigures are $\Delta \text{p}K_{\text{a}} = 0$ and $\text{pI} = 7.0$.

brush, which makes them useful tools for the separation of protein mixtures.[76]

Interestingly, the uptake behavior observed in our simulations is in qualitative agreement with experiments on the selective adsorption of the proteins β-Glucosidase and BSA into a quenched polycationic (PMAETA) and an annealed polycationic brush (PAEMH).[76] As these experiments demonstrated, quenched brushes exhibit a broad pH-window of strong adsorption compared to the narrow window seen in annealed brushes. Also, while the maximum uptake of BSA was found to be comparable in both PMAETA and PAEMH, β-Glucosidase showed a much stronger adsorption into the quenched brush than the annealed one. In line with our previous discussion, this likely happens because PAEMH and BSA have an overlapping window of pH where both are strongly ionized, compared to PAEMH and β-Glucosidase.

3.2.3 Effect of Salt Concentration

In addition to the pH-value, another important control parameter that can be leveraged in experiments is the salt concentration. For example, recent experiments[15] and simulations[52] have shown that changing the salt concentration has a profound influence on the ionization behavior of weak polyelectrolyte brushes. In Fig. 5 (a) we show the uptake of ampholytes with pI = 7.0 into a brush at various bulk salt concentrations. Evidently, the strength of the uptake enhances and the pH window of uptake becomes broader with decreasing salt concentration. Qualitatively, this behavior is already expected on the level of the classical Donnan theory, which predicts that the partitioning of counterions increases as a universal function with the ratio $c_{\mathrm{A}^-}/2I^{\mathrm{res}}$, where c_{A^-} is the concentration of the impermeable ions and I^{res} ionic strength of the reservoir.[33] In the inset of Fig. 5 (a), the ampholyte partitioning is plotted as a function of $c_{\mathrm{A}^-}/2I^{\mathrm{res}}$. For all cases, the partitioning at pH-values below the isoelectric point follows a master curve with $c_{\mathrm{A}^-}/2I^{\mathrm{res}}$, suggesting that in this regime the uptake is predominantly dictated by $c_{\mathrm{A}^-}$and the ionic strength I^{res}. The observed deviations near and above the isoelectric point happen because the charge regulation of the ampholyte becomes a decisive factor in this regime. The dashed pink line is the ideal counterion partitioning predicted by the Donnan theory and is given by $\xi_+ = \frac{c_{\mathrm{A}^-}}{2I^{\mathrm{res}}} + \sqrt{\left(\frac{c_{\mathrm{A}^-}}{2I^{\mathrm{res}}}\right)^2 + 1}$. A similar behavior is observed in the case of quenched brushes (cf. Fig. S6 in the ESI). To explain the broadened pH window of uptake that is observed at lower salt concentrations, we investigate the charge regulation of the ampholyte upon adsorption. Fig. 5 (b) displays the net charge of the ampholyte inside the brush, $z_{\mathrm{amph}}^{\mathrm{brush}}$, estimated from the *local* pH, and the net charge of the ampholyte in the reservoir as a function of the pH in the reservoir. (The net charge of the ampholyte inside the brush calculated explicitly from adsorbed ampholytes is shown in Fig. S7 in the ESI.) It is evident that with decreasing salt concentration, the window beyond the isoelectric point where charge reversal happens, widens. The larger shift seen at low salt concentrations stems from an enhanced lowering of the *local* pH inside the brush at low salt concentrations (shown in Fig. S8) and thus explains the concomitant widening of the uptake win-

dow. Furthermore, as another consequence of this effect, the pH-value at which the maximum uptake happens increases with decreasing salt concentration.

The observed salt-dependent uptake behavior is qualitatively similar to the one observed in experiments on BSA adsorption into weak brushes.[14,26,77] BSA is known to be a protein with a non-patchy, i.e. fairly homogeneous distribution of amino acids, such that charge regulation dominates the adsorption near the isoelectric point. This insight gives a plausible argument why it shares a qualitative resemblance to our simplified ampholyte model.

3.2.4 Effect of Charge Regulation

Until now, we only studied how the uptake changes as external parameters, i.e. the pH-value and the salt concentration are varied. However, in general, the uptake behavior is also profoundly influenced by intrinsic material parameters of the ampholyte such as $\Delta \mathrm{p}K_\mathrm{a}$. Fig. 6 (a) shows the net charge of the ampholyte in the reservoir and the net charge of the ampholyte inside the brush for $\mathrm{pI} = 7$ and a range of $\Delta \mathrm{p}K_\mathrm{a}$ values. The window beyond the isoelectric point where charge reversal of the ampholyte happens remains the same in all the cases. However, even though this shift is invariant, the different slopes of the ionization curves lead to a varying amount of ionization near the isoelectric point. The slopes of the ionization curves can be quantified using the charge regulation capacitance C_z,[10] which is defined as

$$C_z \equiv -\frac{\partial z_\mathrm{amph}^\mathrm{res}}{\partial \left(\ln(10)\,\mathrm{pH}\right)} \tag{15}$$

and shown in Fig. 6 (b). For $\Delta \mathrm{p}K_\mathrm{a} = 0$, the concurrent ionization of the acid and the base leads to a large charge regulation capacitance near the isoelectric point. On the contrary, for $\Delta \mathrm{p}K_\mathrm{a} \gg 0$, a complete decoupling of the ionization of the acid and the base leads to a broad window of pH near the isoelectric point where both remain neutral, rendering the ampholyte overall neutral and leading to a small charge regulation capacitance. Consequently, the observed uptake behavior, shown in Fig 6

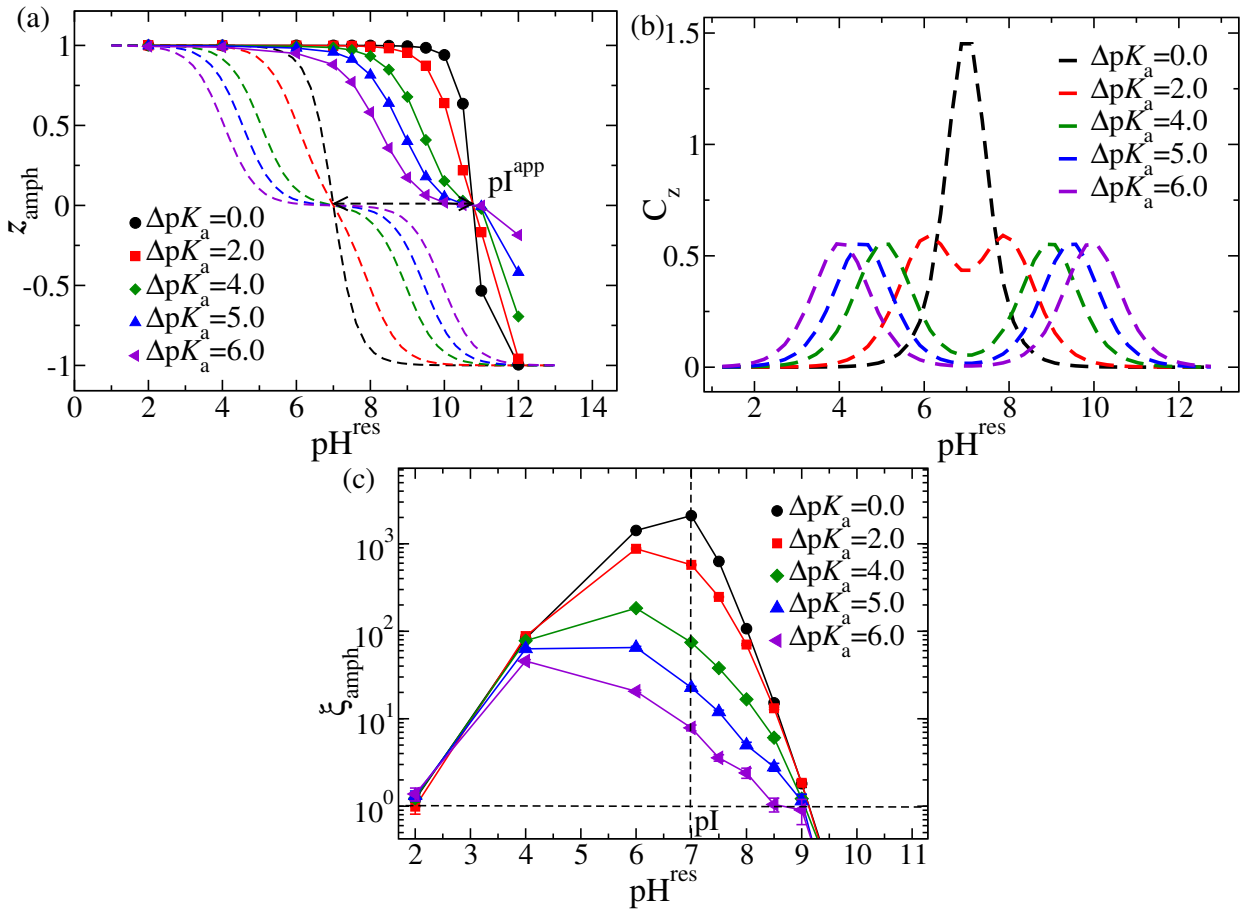

Figure 6: (a): Average net charge of the ampholyte in the reservoir ($z^{\mathrm{res}}_{\mathrm{amph}}$), shown with dashed lines, and average charge of the ampholyte within the brush ($z^{\mathrm{brush}}_{\mathrm{amph}}$), shown with solid symbols, as a function of the pH in the reservoir ($\mathrm{pH}^{\mathrm{res}}$) for a range of different $\Delta \mathrm{p}K_{\mathrm{a}}$ values. (b): Charge regulation capacitance ($\mathrm{C_z}$) of the ampholyte in the reservoir as a function of $\mathrm{pH}^{\mathrm{res}}$for different $\Delta \mathrm{p}K_{\mathrm{a}}$ values. (c): Ampholyte uptake (ξ_{amph}) in an annealed brush as a function of the pH in the reservoir ($\mathrm{pH}^{\mathrm{res}}$) for a range of different $\Delta \mathrm{p}K_{\mathrm{a}}$ values. The parameters chosen in all subfigures are $c_{\mathrm{salt}} = 10^{-4}\,\mathrm{M}$ and $\mathrm{pI} = 7.0$.

(c), is strongly dependent on the value of $\Delta \mathrm{p}K_{\mathrm{a}}$. We observe a maximum uptake strength for the case $\Delta \mathrm{p}K_{\mathrm{a}} = 0$, with the uptake diminishing as $\Delta \mathrm{p}K_{\mathrm{a}}$ increases. This behavior is consistent with the charge regulation capacitance, which is large near the isoelectric point for $\Delta \mathrm{p}K_{\mathrm{a}} = 0$ and subsequently diminishes. Since the charge regulation capacitance directly encodes the ability of the ampholyte to adjust its charge, a large value thus increases the uptake of ampholytes.

The above insight is especially useful for the separation of different proteins with similar isoelectric points but different charge regulation capacitances. For example,

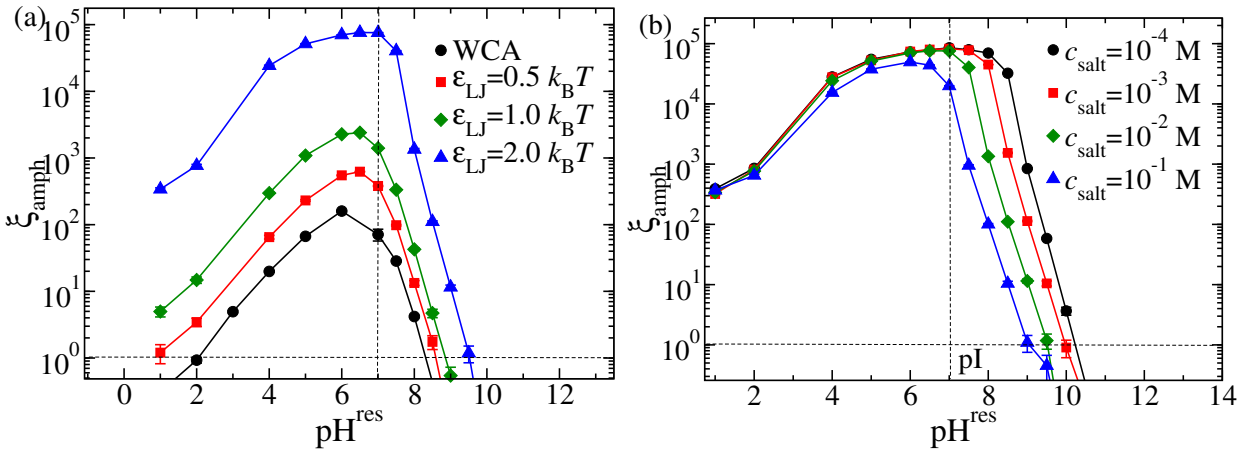

Figure 7: (a): Ampholyte uptake (ξ_{amph}) in an annealed brush as a function of the pH in the reservoir ($\mathrm{pH}^{\mathrm{res}}$) for a range of different non-electrostatic attraction strengths ϵ_{LJ} and a salt concentration of $c_{\mathrm{salt}} = 10^{-2}\,\mathrm{M}$. (b): Ampholyte uptake (ξ_{amph}) in an annealed brush as a function of the pH in the reservoir ($\mathrm{pH}^{\mathrm{res}}$) for a fixed non-electrostatic attraction strength $\epsilon_{\mathrm{LJ}} = 2.0\,k_{\mathrm{B}}T$ and different salt concentrations. The parameters chosen in both subfigures are $\Delta \mathrm{p}K_{\mathrm{a}} = 0$ and $\mathrm{pI} = 7.0$.

the previously mentioned model proteins BSA and β-Glucosidase have very similar isoelectric points (4.4 and 4.9, respectively), but BSA reaches its maximum negative ionization upon adsorption at a lower pH-value than β-Glucosidase.[76] As a result, the maximum uptake of both proteins into a quenched brush (PMAETA) happens at clearly separated pH values, allowing for a selective uptake.

3.2.5 Effect of Non-Electrostatic Attractions

Previous studies stressed the inevitability of including non-electrostatic attractions to quantitatively describe the uptake of BSA into planar brushes observed in experiments.[26] Thus, in this section we address how the inclusion of non-electrostatic short-range attractions influences the uptake behavior of the ampholytes. To model the short-range interactions between the ampholyte and the monomers that comprise the brush, we change the repulsive WCA potential between these particles to a Lennard-Jones potential with an interaction strength ϵ_{LJ}. In Fig. 7 (a) we show the uptake as a function of the reservoir pH for varying interaction strengths ϵ_{LJ} and a salt concentration of $c_{\mathrm{salt}} = 10^{-2}\,\mathrm{M}$. Evidently, the inclusion of short-range attractions enhances the

uptake of ampholytes both below and above the isoelectric point. Our analysis of the PMF for a neutral particle (cf. Fig. S9 in the ESI) shows that by increasing ϵ_{LJ} beyond a value of roughly $k_{\mathrm{B}}T$, non-electrostatic attractive interactions outweigh entropic and volumetric effects within the brush and lead to an enhanced partitioning into the brush. Thus, even in the regime of low pH-values ($\mathrm{pH}^{\mathrm{res}} < 2.0$), where the brush is electroneutral with no relevant electrostatic interactions, a substantial amount of ampholytes is adsorbed for $\epsilon_{\mathrm{LJ}} \gtrsim k_{\mathrm{B}}T$. Fig. 7 (b) shows the effect of salt concentration for the case $\epsilon_{\mathrm{LJ}} = 2.0\, k_{\mathrm{B}}T$. Previously, in the purely repulsive case (Fig. 5 (a)), even for pH-values below the isoelectric point there was a strong dependence of the uptake behavior on the salt concentration. In contrast, here the uptake is nearly independent of the salt concentration in this regime. This happens, because the free energy contribution from the non-electrostatic attraction is dominant over the electrostatic adsorption energy in the regime where the brush is weakly charged. However, for $\mathrm{pH}^{\mathrm{res}} > \mathrm{pI}$, the free energy penalty associated with a charge reversal is high compared to the short range attraction forces, resulting in an electrostatically dominated regime. As a result, with decreasing salt concentration an enhanced window of adsorption is seen beyond the isoelectric point, anaologous to the case without short-range attractions (Fig. 5 (a)).

3.3 Potential of Mean Force for Ampholyte Adsorption

Until now, our analysis neglected the spatially varying structure of the brush, treating brush and bulk solution as a two-phase system. In this section, we employ potential of mean force (PMF) calculations to study the free energy of interaction of an ampholyte with a weak polyelectrolyte brush, fully resolving the spatial inhomogeneity of the system. As explained in the methods section, we use the umbrella sampling technique to calculate the PMF in our simulations. Here, we use a single charge regulating ampholyte as our probe and the distance z between the ampholyte and the grafting surface of the brush as the collective variable. This calculation assumes that the presence of the ampholyte does not noticeably affect the ionic profile or energetics of the system. Since there is only a single ampholyte present in these simulations, in this

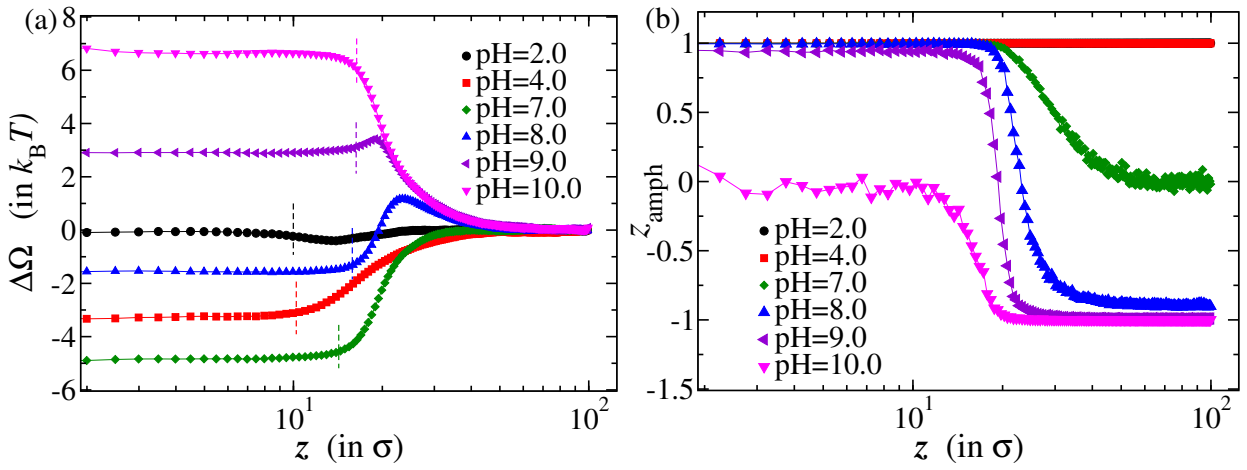

Figure 8: (a): Potential of mean force for an ampholyte ($\Delta\Omega$) as a function of distance from the brush grafting surface (z) for different pH. The dashed lines represent the brush boundary estimated from the average end-to-end distance of the brush polymers. (b): Average net charge of an ampholyte (z_{amph}) as a function of distance from the brush grafting surface (z) for different pH. Parameters chosen are $\mathrm{p}K_{\mathrm{a}}^{\mathrm{acid}} = 7.0$, $\mathrm{p}K_{\mathrm{a}}^{\mathrm{base}} = 7.0$, pI = 7.0, $c_{\mathrm{salt}} = 10^{-2}$M.

case the retrieved free energy of insertion is similar to the case where the concentration of ampholytes in the bulk is negligibly small compared to the other salt ions. The local partition coefficient $\xi_{\mathrm{amph}}(z)$ of ampholytes can be related to the PMF $\Delta\Omega(z)$ by $\xi_{\mathrm{amph}}(z) = \exp(-\beta\Delta\Omega(z))$.

Fig. 8 (a) shows the PMF for a system with pI = 7, $\Delta\mathrm{p}K_{\mathrm{a}} = 0$ and a bulk salt concentration of $c_{\mathrm{salt}} = 10^{-2}$ M at various pH-values. In the case $\mathrm{pH}^{\mathrm{res}} \leq$ pI we observe that the minimum of the PMF lies within the brush, indicating an uptake favorability. Furthermore, the PMF is essentially constant throughout the brush, which results in a nearly uniform distribution of ampholytes within the brush. For larger molecules such as proteins, this might not be the case due to steric effects and one expects a localization at the brush-solution interface.[23,29] An examination of the corresponding z-dependent charge profile of the ampholyte, shown in Fig. 8 (b), reveals that the ampholyte is always completely negatively charged within the brush in the case $\mathrm{pH}^{\mathrm{res}} \leq$ pI. For a pH-value slightly above the isoelectric point ($\mathrm{pH}^{\mathrm{res}} = 8$), we observe that the free energy minimum still lies within the brush, indicating a tendency to take up ampholytes. This uptake is furthermore accompanied by a reversal of the charge from almost fully negative to a fully positively charged state within the brush. Interestingly, in this case

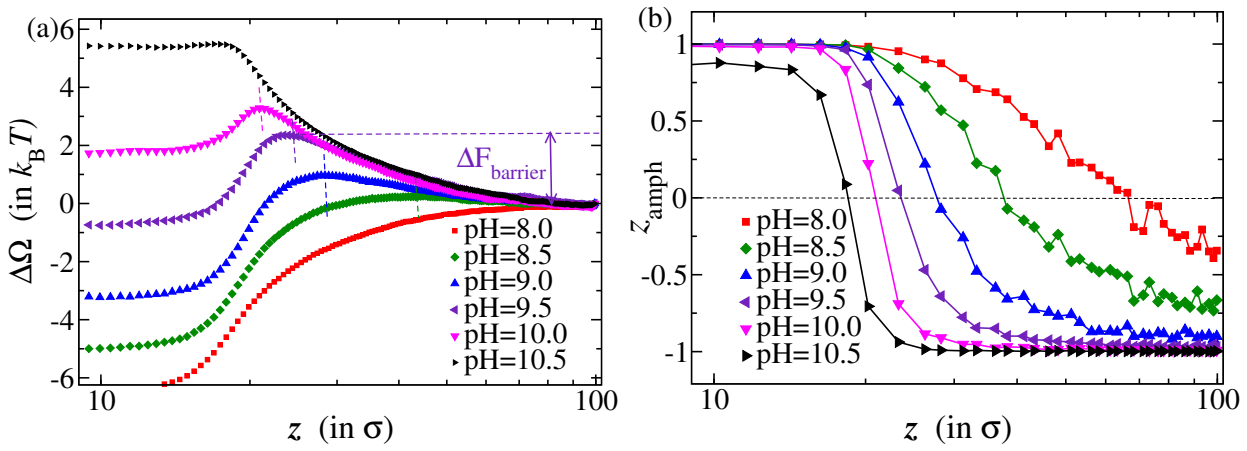

Figure 9: (a): Potential of mean force ($\Delta\Omega$) as a function of distance from the grafting surface (z) for different pH beyond pI for the case of $\Delta \mathrm{p}K_\mathrm{a} = 0$. (b): Average net charge of an ampholyte (z_amph) as a function of distance from the brush grafting surface (z) for different pH beyond pI. Dashed lines in (a) indicate the peak of the potential barrier which overlaps with the zero crossing points in the charge regulation plot in (b). Parameters chosen are $\epsilon_\mathrm{LJ} = 0.0$, $\mathrm{p}K_\mathrm{a}^\mathrm{acid} = 7.0$, $\mathrm{p}K_\mathrm{a}^\mathrm{base} = 7.0$, $\mathrm{pI} = 7.0$, $c_\mathrm{salt} = 10^{-4}$M.

there emerges a free energy barrier that will be discussed below in detail. While this barrier should have no noticeable influence on the equilbrium uptake behavior, it could kinetically hinder the uptake of ampholytes. Finally, for $\mathrm{pH}^\mathrm{res} \gg \mathrm{pI}$ the free energy minimum lies in the solution phase, which indicates that the uptake of ampholytes by the brush is unfavorable in this case. Note that even in this case there happens a (partial) charge reversal as the ion moves into the brush, which is however not sufficient to cause an uptake. This behavior is consistent with our earlier observations above.

3.3.1 Interfacial Free Energy Barrier

In this section we solely focus on the pH regime beyond the isoelectric point, where an interfacial free energy barrier exists. Fig. 9 (a) shows the PMF for a system with $\mathrm{pI} = 7$, $\Delta \mathrm{p}K_\mathrm{a} = 0$ and a bulk salt concentration of $c_\mathrm{salt} = 10^{-4}\,\mathrm{M}$ at various pH-values in the range $8.0 \leq \mathrm{pH}^\mathrm{res} \leq 10.5$. We observe the emergence of an interfacial free energy barrier for $\mathrm{pH}^\mathrm{res} \gtrsim 8.5$ that vanishes again for $\mathrm{pH}^\mathrm{res} \gtrsim 10.5$. Noticeably, as the pH-value is increased, the free energy barrier becomes more prominent and moves closer to the wall. Furthermore, the vanishing of the barrier is related to an increase of the

PMF within the brush. We can explain the emergence of the barrier by investigating the spatially resolved average net charge of the ampholyte, shown in Fig. 9 (b). An examination of the charge profile reveals that the ampholyte regulates its charge as it is moved closer to the brush, ultimately leading to a charge reversal. However, the point of charge reversal, i.e. the distance at which the ampholyte is neutral, depends on the pH-value. Specifically, it moves closer to the wall as the bulk pH-value is increased. This behavior is related to the fact that the z-dependent local pH-profile, $\mathrm{pH}(z)$, changes depending on the pH-value in the bulk solution. As a consequence, the point of charge reversal (i.e the point of zero crossing), defined by $\mathrm{pH}(z) = \mathrm{pI}$, also moves. Consequently, as the ampholyte enters the interactive vicinity of the brush from the solution, it initially retains a negative charge, leading to an overall repulsive interaction that is a seen as the barrier in the PMF. However, once the *local* pH crosses a value of pI, charge reversal happens and the interaction can become energetically favorable. Following this explanation, one expects the maximum of the free energy barrier roughly at the distance where the charge reversal happens. An analysis of the simulation results (Fig. 9 (a)) reveals that this is indeed the case. Besides that, a closer look also reveals that charge reversal itself might not suffice to ensure adsorption at higher pH beyond pI.

For the case $\Delta \mathrm{p}K_\mathrm{a} \gg 0$ (Fig. 10 (a)), no free energy barrier exists. This behavior can be explained by the fact that, in contrast to the previous case, the charge regulation capacitance near the isoelectric point is low. Consequently, even for pH values beyond the pI, the ampholyte charge remains close to zero in the solution, eliminating the barrier that is associated with the free energy cost of charge reversal. Furthermore, an examination of the charge profile (Fig. 10 (b)) reveals that the slow charge regulation near the isoelectric point leads to only a partial charge reversal inside the brush. The partial charge reversal reduces the uptake favorability (i.e., $\Delta\Omega > 0$ inside the brush) as the pH increases beyond the pI. In summary, for $\Delta \mathrm{p}K_\mathrm{a} \approx 0$, despite the presence of a free energy barrier, complete charge reversal occurs. This results in a stronger binding affinity at pH values beyond the pI compared to the case of $\Delta \mathrm{p}K_\mathrm{a} \gg 0$, where

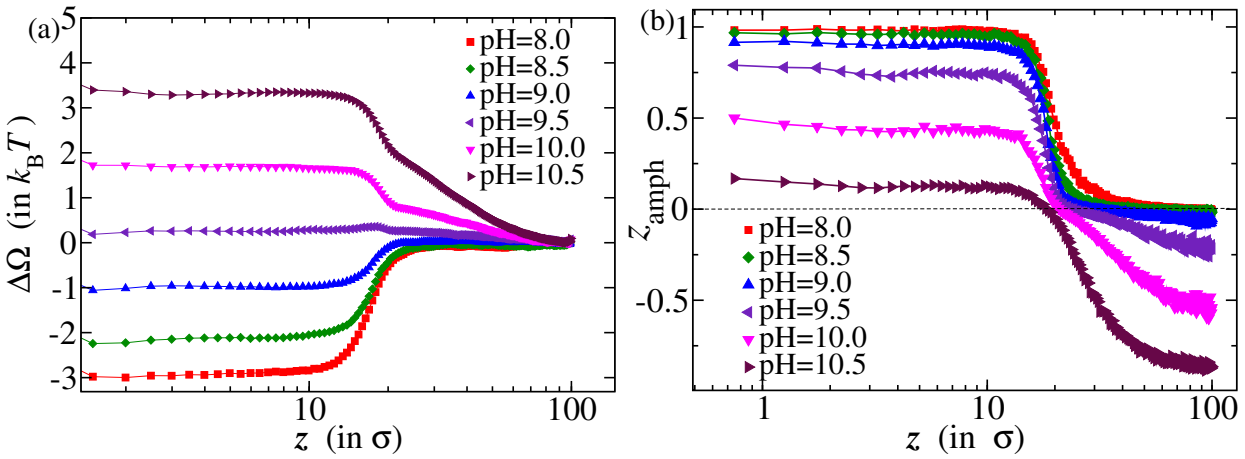

Figure 10: (a): Potential of mean force ($\Delta\Omega$) as a function of distance from the grafting surface (z) for different pH beyond pI for the case of $\Delta \mathrm{p}K_\mathrm{a} = 4.0$. No interfacial free energy barrier is seen. (b): Average net charge of an ampholyte (z_amph) as a function of distance from the brush grafting surface (z) for different pH beyond pI. Parameters chosen are $\epsilon_\mathrm{LJ} = 0.0$, $\mathrm{p}K_\mathrm{a}^\mathrm{acid} = 9.0$, $\mathrm{p}K_\mathrm{a}^\mathrm{base} = 5.0$, $\mathrm{pI} = 7.0$, $c_\mathrm{salt} = 10^{-4}\,\mathrm{M}$.

the absence of the interfacial barrier does not compensate for the limited uptake caused by the partial charge reversal of the ampholyte.

4 Conclusion and Outlook

In this study, we used particle-based simulations to explore how the adjustable response of a weak polyelectrolyte brush, influenced by changes in pH or salt concentration, can regulate the uptake and release of simple toy proteins, here modelled as pH-responsive ampholytes. Using the Grand-Reaction Monte Carlo method, we simulated a two-phase system comprising a weak polyelectrolyte brush coupled to a bulk solution containing salt ions and pH-dependent ampholytes. The enhanced partitioning of protons into the polyanionic brush effectively lowers the pH inside the brush, significantly shifting the ionization of the brush ($\mathrm{p}K_\mathrm{A}^\mathrm{app}$) and the ampholyte upon uptake. The ampholyte undergoes a reionization and charge reversal within a pH window ($\Delta\mathrm{pH} \approx \mathrm{pI}^\mathrm{app} - \mathrm{pI}$) beyond its isoelectric point. This coupling of the ionization state of the brush and the ampholyte has intriguing implications for controlling the uptake behavior.

In quenched brushes, where the brush ionization remains constant, the maximum

uptake strength remains the same for ampholytes of any isoelectric point, with only the pH window shifting accordingly. Conversely, in weak brushes, the coupling of the charge regulation of the brush and the ampholyte leads to a selectivity in uptake that depends on the isoelectric point. For weak brushes with $\mathrm{p}K_\mathrm{A} \ll \mathrm{pI}$, a substantial pH window exists where the brush bears a negative charge while the ampholyte is partially positive ($\mathrm{p}K_\mathrm{A}^\mathrm{app} < \mathrm{pH} < \mathrm{pI}^\mathrm{app}$), resulting in a non-monotonic uptake profile. The maximum uptake strength depends on the maximum ionization state of both the brush and the ampholyte within the overlapping pH window. Thus, in the limit of $\mathrm{p}K_\mathrm{A} \ll \mathrm{pI}$, both the brush and the ampholyte can reach full ionization at the same time, attaining a maximum uptake strength similar to that of quenched brushes. In contrast, in the case $\mathrm{p}K_\mathrm{A} \gtrsim \mathrm{pI}$ no ampholyte uptake occurs at all. To summarize, while quenched brushes exhibit a larger uptake strength than annealed brushes, better selectivity and tunability of protein uptake from a protein mixture are attainable with annealed brushes.[76]

In addition to the pH, our simulations demonstrate that adjusting salt levels is another control parameter that can be leveraged to achieve a tunable response. With decreasing salt concentration, the pH window for charge reversal of the ampholyte widens due to an enhanced lowering of the *local* pH within the brush. This results in a broader uptake window and a shift of the maximum uptake towards a higher pH-value. Thus, at a fixed pH-value beyond the isoelectric point, adding more salt to the bulk solution can lead to a complete desorption of an ampholyte from the brush. The overall behavior observed in our simulations is *qualitatively* similar to experimental observations of BSA adsorption into weak brushes,[14,26,77] where charge regulation plays a governing role, as demonstrated by de Vos et al.[26] This highlights the protein's adjustment of its charge in response to the brush's potential, even on the "wrong side" of its isoelectric point (pI), emphasizing the importance of charge regulation in protein-brush interactions.

Further, our study demonstrates that the charge regulation capacitance of the ampholyte profoundly influences its binding affinity. Ampholytes with a comparatively

high charge regulation capacitance near the isoelectric point ($\Delta \mathrm{p}K_\mathrm{a} \approx 0$) can achieve significant adsorption across a wider pH range beyond the isoelectric point.[30] Although there is a free energy barrier due to the reionization cost of the ampholyte upon uptake, the complete charge reversal due to steeper charge regulation near the pI favors stronger adsorption. In contrast, ampholytes with low charge regulation capacitance near the isoelectric point ($\Delta \mathrm{p}K_\mathrm{a} \gg 0$) do not encounter a free energy barrier, but their uptake is limited by partial charge reversal. Overall, ampholytes with $\Delta \mathrm{p}K_\mathrm{a} \approx 0$ exhibit stronger uptake for any given pH compared to those with $\Delta \mathrm{p}K_\mathrm{a} \gg 0$. This observation is in qualitative agreement with experiments on the proteins BSA and β-Glucosidase,[76] which share similar isoelectric points but differ in their charge regulation capacitances. Because BSA reaches a substantial negative ionization at a lower pH than β-Glucosidase, the uptake peaks of the two proteins occur at distinctly different pH values and vary in strength, allowing for selective separation. Besides that, a closer look at the potential of mean force also reveals that with increasing pH beyond pI, charge reversal itself might not suffice to ensure adsorption.

Further, our study suggests that non-electrostatic short range attractions broaden the window of uptake both below and above the pI. Also, increasing the short range attraction strength reduces the pH sensitivity at lower pH values, where electrostatic interactions play a minor role, in contrast to higher pH-values, where the electrostatic energy cost involved leads to discernible differences in the uptake strength. Additionally, brush grafting density is another control parameter that profoundly influences the uptake window of ampholytes (see ESI Section 9).

The present work primarily addresses the pH-response of weak polyelectrolyte brushes and its coupling with charge regulating ampholytes as a function of various environmental and intrinsic parameters. Our simple coarse-grained model isolates and examines the explicit role of monopolar charge regulation of an ampholyte under the interactive influence of the brush and will serve as a useful reference when studying more complex protein models. Interestingly, most of our findings are consistent with experimental results on non-patchy proteins like BSA,[14,26,77] suggesting that in these

cases charge regulation plays a dominant role in the uptake by polyelectrolyte brushes. Nevertheless, it is obvious that assessing protein behavior within the context of the interaction with brushes requires consideration of various factors beyond charge regulation alone, such as the specific distribution of dissociable groups on the protein surface, leading to higher multipole moments,[22,23,27] non-electrostatic attractive interactions,[26] and even volumetric contributions.[29] All of these points will be addressed explicitly in our follow-up work.

Overall, our results demonstrate the potential of tuning the uptake properties of ampholytic entities into weak polyelectrolyte brushes by manipulating external parameters, providing valuable insights for designing responsive interfaces with specific adsorption characteristics. These findings can aid in the development of advanced separation techniques,[76] targeted drug delivery systems[78–80] and smart filtration technologies,[50,51] where precise control over uptake and release of proteins or enzymes is crucial.

5 Acknowledgments

K.R. and C.H. acknowledge the German Research Foundation (DFG) for funding through grant 451980436 and 429529433. D.B. and C.H. acknowledge the DFG for funding within the Research Unit FOR2811 "Adaptive Polymer Gels with Model Network Structure" under grant 423791428 along with grant 397384169 (TP7). We also acknowledge funding from the DFG Compute Cluster grant 492175459. We thank Peter Košovan for helpful discussions.

References

(1) Landsgesell, J.; Nová, L.; Rud, O.; Uhlík, F.; Sean, D.; Hebbeker, P.; Holm, C.; Košovan, P. Simulations of ionization equilibria in weak polyelectrolyte solutions and gels. *Soft Matter* **2019**, *15*, 1155–1185, DOI: 10.1039/C8SM02085J.

(2) Peppas, N. A.; Bures, P.; Leobandung, W.; Ichikawa, H. Hydrogels in pharmaceutical formulations. *European journal of pharmaceutics and biopharmaceutics* **2000**, *50*, 27–46, DOI: 10.1016/S0939-6411(00)00090-4.

(3) Jia, X.; Kiick, K. L. Hybrid multicomponent hydrogels for tissue engineering. *Macromolecular bioscience* **2009**, *9*, 140–156, DOI: 10.1002/mabi.200800284.

(4) Jagur-Grodzinski, J. Polymeric gels and hydrogels for biomedical and pharmaceutical applications. *Polymers for Advanced Technologies* **2010**, *21*, 27–47, DOI: 10.1002/pat.1504.

(5) Tang, J.; Katashima, T.; Li, X.; Mitsukami, Y.; Yokoyama, Y.; Sakumichi, N.; Chung, U.-i.; Shibayama, M.; Sakai, T. Swelling Behaviors of Hydrogels with Alternating Neutral/Highly Charged Sequences. *Macromolecules* **2020**, *53*, 8244–8254, DOI: 10.1021/acs.macromol.0c01221.

(6) Landsgesell, J.; Beyer, D.; Hebbeker, P.; Košovan, P.; Holm, C. The pH-Dependent Swelling of Weak Polyelectrolyte Hydrogels Modeled at Different Levels of Resolution. *Macromolecules* **2022**, *55*, 3176–3188, DOI: 10.1021/acs.macromol.1c02489.

(7) Beyer, D.; Košovan, P.; Holm, C. Simulations explain the Swelling Behavior of Hydrogels with Alternating Neutral and Weakly Acidic Blocks. *Macromolecules* **2022**, *55*, 10751–10760, DOI: 10.1021/acs.macromol.2c01916.

(8) Staňo, R.; Košovan, P.; Tagliabue, A.; Holm, C. Electrostatically Cross-Linked Reversible Gels—Effects of pH and Ionic Strength. *Macromolecules* **2021**, *54*, 4769–4781, DOI: 10.1021/acs.macromol.1c00470.

(9) Rud, O. V.; Landsgesell, J.; Holm, C.; Košovan, P. Modeling of weak polyelectrolyte hydrogels under compression – Implications for water desalination. *Desalination* **2021**, *506*, 114995, DOI: 10.1016/j.desal.2021.114995.

(10) Lund, M.; Jönsson, B. On the Charge Regulation of Proteins. *Biochemistry* **2005**, *44*, 5722–5727, DOI: 10.1021/bi047630o.

(11) Lund, M.; Jönsson, B. Charge regulation in biomolecular solution. *Quarterly reviews of biophysics* **2013**, *46*, 265–281, DOI: 10.1017/S003358351300005X.

(12) Torres, P. B.; Quiroga, E.; Ramirez-Pastor, A. J.; Boeris, V.; Narambuena, C. F. Interaction between β-Lactoglobuline and Weak Polyelectrolyte Chains: A Study Using Monte Carlo Simulation. *The Journal of Physical Chemistry B* **2019**, *123*, 8617–8627, DOI: 10.1021/acs.jpcb.9b03276.

(13) Svirelis, J.; Adali, Z.; Emilsson, G.; Medin, J.; Andersson, J.; Vattikunta, R.; Hulander, M.; Järlebark, J.; Kolman, K.; Olsson, O., et al. Stable trapping of multiple proteins at physiological conditions using nanoscale chambers with macromolecular gates. *Nature Communications* **2023**, *14*, 5131, DOI: 10.1038/s41467-023-40889-4.

(14) Wittemann, A.; Haupt, B.; Ballauff, M. Adsorption of proteins on spherical polyelectrolyte brushes in aqueous solution. *Physical Chemistry Chemical Physics* **2003**, *5*, 1671–1677, DOI: 10.1039/B300607G.

(15) Ferrand-Drake del Castillo, G.; Hailes, R. L. N.; Dahlin, A. Large Changes in Protonation of Weak Polyelectrolyte Brushes with Salt Concentration – Implication for Protein Immobilization. *The Journal of Physical Chemistry Letters* **2020**, *11*, 5212–5218, DOI: 10.1021/acs.jpclett.0c01289.

(16) Wittemann, A.; Ballauff, M. Interaction of proteins with linear polyelectrolytes and spherical polyelectrolyte brushes in aqueous solution. *Physical Chemistry Chemical Physics* **2006**, *8*, 5269–5275, DOI: 10.1039/B609879G.

(17) Walkowiak, J.; Gradzielski, M.; Zauscher, S.; Ballauff, M. Interaction of proteins with a planar poly (acrylic acid) brush: analysis by quartz crystal mi-

crobalance with dissipation monitoring (QCM-D). *Polymers* **2020**, *13*, 122, DOI: 10.3390/polym13010122.

(18) Ferrand-Drake del Castillo, G.; Hailes, R. L. N.; Adali-Kaya, Z.; Robson, T.; Dahlin, A. Generic high-capacity protein capture and release by pH control. *Chemical Communications* **2020**, *56*, 5889–5892, DOI: 10.1039/D0CC01250E.

(19) del Castillo, G. F.-D.; Kyriakidou, M.; Adali, Z.; Xiong, K.; Hailes, R. L.; Dahlin, A. Electrically switchable polymer brushes for protein capture and release in biological environments. *Angewandte Chemie International Edition* **2022**, *61*, e202115745, DOI: 10.1002/anie.202115745.

(20) Xu, X.; Angioletti-Uberti, S.; Lu, Y.; Dzubiella, J.; Ballauff, M. Interaction of proteins with polyelectrolytes: Comparison of theory to experiment. *Langmuir* **2018**, *35*, 5373–5391, DOI: 10.1021/acs.langmuir.8b01802.

(21) Becker, A. L.; Henzler, K.; Welsch, N.; Ballauff, M.; Borisov, O. Proteins and polyelectrolytes: A charged relationship. *Current Opinion in Colloid & Interface Science* **2012**, *17*, 90–96, DOI: 10.1016/j.cocis.2011.10.001.

(22) Yigit, C.; Heyda, J.; Ballauff, M.; Dzubiella, J. Like-charged protein-polyelectrolyte complexation driven by charge patches. *The Journal of Chemical Physics* **2015**, *143*, DOI: 10.1063/1.4928078.

(23) Yigit, C.; Kanduc, M.; Ballauff, M.; Dzubiella, J. Interaction of charged patchy protein models with like-charged polyelectrolyte brushes. *Langmuir* **2017**, *33*, 417–427, DOI: 10.1021/acs.langmuir.6b03797.

(24) Leermakers, F.; Ballauff, M.; Borisov, O. On the mechanism of uptake of globular proteins by polyelectrolyte brushes: A two-gradient self-consistent field analysis. *Langmuir* **2007**, *23*, 3937–3946, DOI: 10.1021/la0632777.

(25) Biesheuvel, P. M.; Wittemann, A. A modified box model including charge regulation for protein adsorption in a spherical polyelectrolyte brush. *The Journal of Physical Chemistry B* **2005**, *109*, 4209–4214, DOI: 10.1021/jp0452812.

(26) de Vos, W. M.; Biesheuvel, P. M.; de Keizer, A.; Kleijn, J. M.; Cohen Stuart, M. A. Adsorption of the protein bovine serum albumin in a planar poly (acrylic acid) brush layer as measured by optical reflectometry. *Langmuir* **2008**, *24*, 6575–6584, DOI: 10.1021/la8006469.

(27) De Vos, W. M.; Leermakers, F. A.; De Keizer, A.; Cohen Stuart, M. A.; Kleijn, J. M. Field theoretical analysis of driving forces for the uptake of proteins by like-charged polyelectrolyte brushes: Effects of charge regulation and patchiness. *Langmuir* **2010**, *26*, 249–259, DOI: 10.1021/la902079u.

(28) Popova, T. O.; Zhulina, E. B.; Borisov, O. V. Interaction of Polyanionic and Polycationic Brushes with Globular Proteins and Protein-like Nanocolloids. *Biomimetics* **2023**, *8*, 597, DOI: 10.3390/biomimetics8080597.

(29) Popova, T. O.; Borisov, O. V.; Zhulina, E. B. Polyelectrolyte Brushes with Protein-Like Nanocolloids. *Langmuir* **2024**, *40*, 1232–1246, DOI: 10.1021/acs.langmuir.3c02556.

(30) Salamatova, T. O.; Zhulina, E. B.; Borisov, O. V. Bovine Serum Albumin interaction with polyanionic and Polycationic brushes: the case theoretical study. *International Journal of Molecular Sciences* **2023**, *24*, 3395, DOI: 10.3390/ijms24043395.

(31) Salamatova, T. O.; Laktionov, M. Y.; Zhulina, E. B.; Borisov, O. V. Polyelectrolyte Brush Interacting with Ampholytic Nanoparticles as Coarse-Grained Models of Globular Proteins: Poisson–Boltzmann Theory. *Biomacromolecules* **2023**, *24*, 2433–2446, DOI: 10.1021/acs.biomac.2c01153.

(32) Lunkad, R.; Barroso da Silva, F. L.; Kosovan, P. Both charge-regulation and

charge-patch distribution can drive adsorption on the wrong side of the isoelectric point. *Journal of the American Chemical Society* **2022**, *144*, 1813–1825, DOI: 10.1021/jacs.1c11676.

(33) Landsgesell, J.; Hebbeker, P.; Rud, O.; Lunkad, R.; Košovan, P.; Holm, C. Grand-Reaction Method for Simulations of Ionization Equilibria Coupled to Ion Partitioning. *Macromolecules* **2020**, *53*, 3007–3020, DOI: 10.1021/acs.macromol.0c00260.

(34) Nap, R.; Gong, P.; Szleifer, I. Weak polyelectrolytes tethered to surfaces: Effect of geometry, acid-base equilibrium and electrical permittivity. *Journal of Polymer Science Part B: Polymer Physics* **2006**, *44*, 2638–2662, DOI: 10.1002/polb.20896.

(35) Nap, R. J.; Tagliazucchi, M.; Szleifer, I. Born energy, acid-base equilibrium, structure and interactions of end-grafted weak polyelectrolyte layers. *The Journal of Chemical Physics* **2014**, *140*, 024910, DOI: 10.1063/1.4861048.

(36) Nap, R. J.; Tagliazucchi, M.; Solveyra, E. G.; Ren, C. L.; Uline, M. J.; Szleifer, I. *Polymer and Biopolymer Brushes: For Materials Science and Biotechnology*; Wiley Blackwell, 2017; pp 161–221.

(37) Zhulina, E. B.; Borisov, O. V. Poisson–Boltzmann Theory of pH-Sensitive (Annealing) Polyelectrolyte Brush. *Langmuir* **2011**, *27*, 10615–10633, DOI: 10.1021/la201456a.

(38) Zhulina, E.; Leermakers, F.; Borisov, O. *Polymer and Biopolymer Brushes: For Materials Science and Biotechnology*; Wiley-Blackwell, 2017; pp 223–241.

(39) Léonforte, F.; Welling, U.; Müller, M. Single-chain-in-mean-field simulations of weak polyelectrolyte brushes. *The Journal of Chemical Physics* **2016**, *145*, 224902, DOI: 10.1063/1.4971212.

(40) Israëls, R.; Leermakers, F. A. M.; Fleer, G. J. On the Theory of Grafted Weak Polyacids. *Macromolecules* **1994**, *27*, 3087–3093, DOI: 10.1021/ma00089a028.

(41) Israëls, R.; Leermakers, F. A. M.; Fleer, G. J.; Zhulina, E. B. Charged Polymeric Brushes: Structure and Scaling Relations. *Macromolecules* **1994**, *27*, 3249–3261, DOI: 10.1021/ma00090a018.

(42) Grosberg, A. Y.; Nguyen, T. T.; Shklovskii, B. I. Colloquium: The physics of charge inversion in chemical and biological systems. *Reviews of Modern Physics* **2002**, *74*, 329, DOI: 10.1103/RevModPhys.74.329.

(43) Rouzina, I.; Bloomfield, V. A. Macroion attraction due to electrostatic correlation between screening counterions. 1. Mobile surface-adsorbed ions and diffuse ion cloud. *Journal of Physical Chemistry* **1996**, *100*, 9977–9989, DOI: 10.1021/jp960458g.

(44) Netz, R. R. Electrostatistics of counter-ions at and between planar charged walls: From Poisson-Boltzmann to the strong-coupling theory. *European Physical Journal E* **2001**, *5*, 557–574, DOI: 10.1007/s101890170039.

(45) Boroudjerdi, H.; Kim, Y.-W.; Naji, A.; Netz, R. R.; Schlagberger, X.; Serr, A. Statics and dynamics of strongly charged soft matter. *Physics Reports* **2005**, *416*, 129–199, DOI: 10.1016/j.physrep.2005.06.006.

(46) Deserno, M.; Holm, C.; May, S. Fraction of Condensed Counterions around a Charged Rod: Comparison of Poisson-Boltzmann Theory and Computer Simulations. *Macromolecules* **2000**, *33*, 199–206, DOI: 10.1021/ma990897o.

(47) Moreira, A. G.; Netz, R. R. Strong-coupling theory for counter-ion distributions. *Europhysics Letters* **2000**, *52*, 705–711, DOI: 10.1209/epl/i2000-00495-1.

(48) Staňo, R.; Nová, L.; Uhlík, F.; Košovan, P. Multivalent counterions accumulate in star-like polyelectrolytes and collapse the polymer in spite of increasing its ionization. *Soft Matter* **2020**, *16*, 1047–1055, DOI: 10.1039/c9sm02318f.

(49) Beyer, D.; Holm, C. Unexpected Two-Stage Swelling of Weak Polyelectrolyte Brushes with Divalent Counterions. *ChemRxiv preprint* **2024**, DOI: 10.26434/chemrxiv-2024-xxjr1.

(50) del Castillo, G. F.-D.; Kyriakidou, M.; Adali, Z.; Xiong, K.; Hailes, R. L.; Dahlin, A. Electrically switchable polymer brushes for protein capture and release in biological environments. *Angewandte Chemie International Edition* **2022**, *61*, e202115745.

(51) Ferrand-Drake del Castillo, G.; Koenig, M.; Müller, M.; Eichhorn, K.-J.; Stamm, M.; Uhlmann, P.; Dahlin, A. Enzyme immobilization in polyelectrolyte brushes: High loading and enhanced activity compared to monolayers. *Langmuir* **2019**, *35*, 3479–3489, DOI: 10.1021/acs.langmuir.9b00056.

(52) Beyer, D.; Košovan, P.; Holm, C. Explaining Giant Apparent pK_{a} Shifts in Weak Polyelectrolyte Brushes. *Physical Review Letters* **2023**, *131*, 168101, DOI: 10.1103/PhysRevLett.131.168101.

(53) Weik, F.; Weeber, R.; Szuttor, K.; Breitsprecher, K.; de Graaf, J.; Kuron, M.; Landsgesell, J.; Menke, H.; Sean, D.; Holm, C. ESPResSo 4.0 – an extensible software package for simulating soft matter systems. *European Physical Journal Special Topics* **2019**, *227*, 1789–1816, DOI: 10.1140/epjst/e2019-800186-9.

(54) Weeber, R.; Grad, J.-N.; Beyer, D.; Blanco, P. M.; Kreissl, P.; Reinauer, A.; Tischler, I.; Košovan, P.; Holm, C. In *Comprehensive Computational Chemistry*, 1st ed.; Yáñez, M., Boyd, R. J., Eds.; Elsevier: Oxford, 2024; pp 578–601, DOI: 10.1016/B978-0-12-821978-2.00103-3.

(55) Grest, G. S.; Kremer, K. Molecular dynamics simulation for polymers in the presence of a heat bath. *Physical Review A* **1986**, *33*, 3628–31, DOI: 10.1103/PhysRevA.33.3628.

(56) Weeks, J. D.; Chandler, D.; Andersen, H. C. Role of Repulsive Forces in Determining the Equilibrium Structure of Simple Liquids. *The Journal of Chemical Physics* **1971**, *54*, 5237–5247, DOI: 10.1063/1.1674820.

(57) Deserno, M.; Holm, C. How to mesh up Ewald sums. I. A theoretical and numerical comparison of various particle mesh routines. *The Journal of Chemical Physics* **1998**, *109*, 7678, DOI: 10.1063/1.477414.

(58) Deserno, M.; Holm, C. How to mesh up Ewald sums. II. An accurate error estimate for the Particle–Particle–Particle-Mesh algorithm. *The Journal of Chemical Physics* **1998**, *109*, 7694, DOI: 10.1063/1.477415.

(59) Arnold, A.; de Joannis, J.; Holm, C. Electrostatics in Periodic Slab Geometries. I. *The Journal of Chemical Physics* **2002**, *117*, 2496–2502, DOI: 10.1063/1.1491955.

(60) de Joannis, J.; Arnold, A.; Holm, C. Electrostatics in Periodic Slab Geometries. II. *The Journal of Chemical Physics* **2002**, *117*, 2503–2512, DOI: 10.1063/1.1491954.

(61) Frenkel, D.; Smit, B. *Understanding Molecular Simulation: From Algorithms to Applications*, 2nd ed.; Computational Science; Academic Press: San Diego, 2002; Vol. 1; DOI: 10.1016/B978-0-12-267351-1.X5000-7.

(62) Reed, C. E.; Reed, W. F. Monte Carlo study of titration of linear polyelectrolytes. *The Journal of Chemical Physics* **1992**, *96*, 1609–1620, DOI: 10.1063/1.462145.

(63) Smith, W. R.; Triska, B. The reaction ensemble method for the computer simulation of chemical and phase equilibria. I. Theory and basic examples. *The Journal of Chemical Physics* **1994**, *100*, 3019–3027, DOI: 10.1063/1.466443.

(64) Johnson, J. K.; Panagiotopoulos, A. Z.; Gubbins, K. E. Reactive canonical Monte Carlo: A new simulation technique for reacting or associating fluids. *Molecular Physics* **1994**, *81*, 717–733, DOI: 10.1080/00268979400100481.

(65) Landsgesell, J.; Holm, C.; Smiatek, J. Wang–Landau Reaction Ensemble Method: Simulation of Weak Polyelectrolytes and General Acid-Base Reactions. *Journal of Chemical Theory and Computation* **2017**, *13*, 852–862, DOI: 10.1021/acs.jctc.6b00791.

(66) Curk, T.; Yuan, J.; Luijten, E. Accelerated simulation method for charge regulation effects. *The Journal of Chemical Physics* **2022**, *156*, 044122, DOI: 10.1063/5.0066432.

(67) Beyer, D.; Holm, C. A generalized grand-reaction method for modeling the exchange of weak (polyprotic) acids between a solution and a weak polyelectrolyte phase. *The Journal of Chemical Physics* **2023**, *159*, 014905, DOI: 10.1063/5.0155973.

(68) Beyer, D.; Landsgesell, J.; Hebbeker, P.; Rud, O.; Lunkad, R.; Košovan, P.; Holm, C. Correction to "Grand-Reaction Method for Simulations of Ionization Equilibria Coupled to Ion Partitioning". *Macromolecules* **2022**, *55*, 1088, DOI: 10.1021/acs.macromol.1c02672.

(69) Staňo, R.; van Lente, J. J.; Lindhoud, S.; Košovan, P. Sequestration of Small Ions and Weak Acids and Bases by a Polyelectrolyte Complex Studied by Simulation and Experiment. *Macromolecules* **2024**, DOI: 10.1021/acs.macromol.3c01209.

(70) Yuan, X.; Hatch, H. W.; Conrad, J. C.; Marciel, A. B.; Palmer, J. C. pH response of sequence-controlled polyampholyte brushes. *Soft Matter* **2023**, *19*, 4333–4344, DOI: 10.1039/D3SM00447C.

(71) Yuan, J.; Wang, Y. Conformation and Ionization Behavior of Charge-Regulating Polyelectrolyte Brushes in a Poor Solvent. *The Journal of Physical Chemistry B* **2021**, *125*, 10589–10596, DOI: 10.1021/acs.jpcb.1c04451.

(72) Torrie, G. M.; Valleau, J. P. Non-Physical Sampling Distributions In Monte-Carlo

Free-Energy Estimation - Umbrella Sampling. *Journal of Computational Physics* **1977**, *23*, 187–199, DOI: 10.1016/0021-9991(77)90121-8.

(73) Kästner, J. Umbrella sampling. *Wiley Interdisciplinary Reviews: Computational Molecular Science* **2011**, *1*, 932–942, DOI: 10.1002/wcms.66.

(74) Kumar, S.; Rosenberg, J. M.; Bouzida, D.; Swendsen, R. H.; Kollman, P. A. The weighted histogram analysis method for free-energy calculations on biomolecules. I. The method. *Journal of Computational Chemistry* **1992**, *13*, 1011–1021, DOI: 10.1002/jcc.540130812.

(75) Grossfield, A. WHAM: the weighted histogram analysis method. 2023; http://membrane.urmc.rochester.edu/wordpress/?page_id=126, version 2.0.10.

(76) Ye, Z.; Li, L.; Dai, L.; Wang, Y.; Yang, Q.; von Klitzing, R.; Guo, X. Selective uptake of different proteins by annealed and quenched cationic spherical polyelectrolyte brushes. *Journal of Polymer Science* **2020**, *58*, 3018–3030, DOI: 10.1002/pol.20200547.

(77) Seyrek, E.; Dubin, P. L.; Tribet, C.; Gamble, E. A. Ionic strength dependence of protein-polyelectrolyte interactions. *Biomacromolecules* **2003**, *4*, 273–282, DOI: 10.1021/bm025664a.

(78) Motornov, M.; Tam, T. K.; Pita, M.; Tokarev, I.; Katz, E.; Minko, S. Switchable selectivity for gating ion transport with mixed polyelectrolyte brushes: approaching 'smart'drug delivery systems. *Nanotechnology* **2009**, *20*, 434006, DOI: 10.1088/0957-4484/20/43/434006.

(79) Zhang, X.; Yang, P.; Dai, Y.; Ma, P.; Li, X.; Cheng, Z.; Hou, Z.; Kang, X.; Li, C.; Lin, J. Multifunctional Up-converting nanocomposites with smart polymer brushes gated mesopores for cell imaging and thermo/pH dual-responsive drug controlled release. *Advanced Functional Materials* **2013**, *23*, 4067–4078, DOI: 10.1002/adfm.201300136.

(80) Zhang, L.; Bei, H. P.; Piao, Y.; Wang, Y.; Yang, M.; Zhao, X. Polymer-brush-grafted mesoporous silica nanoparticles for triggered drug delivery. *ChemPhysChem* **2018**, *19*, 1956–1964, DOI: 10.1002/cphc.201800018.

TOC Graphic